

1 **Spatial-temporal changes in flow hydraulic characteristics and soil loss**
2 **during gully headcut erosion under controlled conditions**

3
4 Mingming Guo^a, Zhuoxin Chen^b, Wenlong Wang^{b,c,*}, Tianchao Wang^d, Qianhua Shi^b, Hongliang
5 Kang^b, Man Zhao^b, Lanqian Feng^c

6
7 a Key laboratory of Mollisols Agroecology, Northeast Institute of Geography and Agroecology,
8 Chinese Academy of Sciences, Harbin 150081, Heilongjiang, China

9 b State Key Laboratory of Soil Erosion and Dryland Farming on the Loess Plateau, Institute of Water
10 and Soil Conservation, Northwest A&F University, Yangling, Shaanxi 712100, China

11 c Institute of Soil and Water Conservation, Chinese Academy of Sciences and Ministry of Water
12 Resources, Yangling, Shaanxi 712100, China

13 d Ulanyab Grassland Station, Jining, Inner Mongolia 012000, China

14 ***Corresponding author:** Wenlong Wang

15 E-mail addresses: nwafu_wwl@163.com; wllwang@nwsuaf.edu.cn

16

17 **Abstract**

18 The temporal-spatial changes in flow hydraulics and energy consumption and their associated soil
19 erosion remain unclear during gully headcut retreat. A simulated scouring experiment was conducted
20 on five headcut plots consisting of upstream area (UA), gully headwall (GH) and gully bed (GB) to
21 elucidate the temporal-spatial changes in flow hydraulic, energy consumption, and soil loss during
22 headcut erosion. The flow velocity at the brink of headcut increased as a power function of time,
23 whereas the jet velocity entry to plunge pool and jet shear stress logarithmically or linearly decreased
24 over time. The jet properties were significantly affected by upstream flow discharge. The Reynold
25 number, runoff shear stress, and stream power of UA and GB increased as logarithmic or power
26 functions of time, but the Froude number decreased logarithmically over time. The Reynold number,
27 shear stress and stream power decreased by 56.0%, 63.8% and 55.9%, respectively, but the Froude
28 number increased by 7.9% when flow dropped from UA to GB. The accumulated energy consumption
29 of UA, GH and GB positions linearly increased with time. 91.12% - 99.90% of total flow energy was
30 consumed during headcut erosion, of which the gully head accounted for 77.7% of total energy
31 dissipation followed by UA (18.3%) and GB (4.0%). The soil loss rate of the “UA-GH-GB” system
32 initially rose and then gradually declined and levelled off. The soil loss of UA and GH decreased
33 logarithmically over time, whereas the GB was mainly characterized by sediment deposition. The
34 proportion of soil loss at UA and GH are 11.5% and 88.5%, respectively, of which the proportion of
35 deposited sediment on GB reached 3.8%. The change in soil loss of UA, GH and GB was significantly
36 affected by flow hydraulic and jet properties. The critical energy consumption initiating soil erosion
37 of UA, GH, and GB are 1.62 J s^{-1} , 5.79 J s^{-1} and 1.64 J s^{-1} , respectively. These results are helpful to
38 deepen the understanding of gully erosion process and hydrodynamic mechanism and also can provide
39 scientific basis for the construction of gully erosion model and the design of gully erosion prevention
40 measures.

41
42 **Keywords:** Gully erosion; Hydraulic property; Headcut retreat; Mass failure; Energy dissipation

43

44 **1 Introduction**

45 Gully erosion is a typical soil erosion process whereby concentrated runoff from an upstream
46 drainage area recurs in a channel and erodes soil from the area through which runoff passed to
47 considerable depth (Poesen et al., 2003; Zhu, 2012). Gully erosion is recognized as the main sediment
48 source in some hilly and gully-dominated watersheds (Poesen et al., 2003; Valentin et al., 2005;
49 Dotterweich et al., 2012). Poesen et al. (2003) reported that soil loss amount caused by gully erosion
50 accounts for 10% - 94% of total soil loss amount based on the collected data from published articles.
51 Moreover, gully erosion can severely damage to infrastructure, enhance the terrain fragmentation, and
52 cause ecosystem instability, land degradation and food safety (Vanmaercke et al, 2016; Zhang et al.,
53 2018; Hosseinalizadeh et al., 2019; Arabameri et al., 2020; Bogale et al., 2020; Belayneh et al., 2020;
54 Wen et al., 2020).

55 As the primary process of the gully erosion, the gully headcut retreat often significantly influences
56 and determines gully erosion (Oostwoud-Wijdenes et al., 2000; Vandekerckhove et al., 2003; Guo et
57 al., 2019). A headcut is defined as a vertical or near-vertical drop or discontinuity on the bed of a gully
58 occurring where flow is concentrated at a knickpoint (Hanson et al., 2001; Bennett et al., 2000). Many
59 studies have demonstrated that the gully erosion is the result of the combined actions of plunge pool
60 erosion by jet flow, upstream runoff incision, headwall erosion by on-wall flow, mass failure of gully
61 head and wall collapse (Vanmaercke et al., 2016; Addisie et al., 2017; Guo et al., 2019). Once a headcut
62 is formed in upstream area, the gully will develop rapidly and not stop forward until a critical
63 topographic condition is formed ($S \leq a \cdot A^b$, where S and A is the slope gradient and drainage area
64 upstream gully headcut, respectively) (Kirkby et al., 2003). Moreover, the different landform units
65 (upstream area, UA; gully head, GH; gully bed, GB) of gully system exhibited completely different
66 erosion processes and hydrodynamic mechanisms during gully headcut erosion (Zhang et al., 2018;
67 Guo et al., 2019; Shi et al., 2020a). The combination and interaction of erosion processes of the three
68 landform units determined gully headcut erosion process (Vanmaercke et al., 2016). Therefore,
69 clarifying the soil erosion process and characteristics of the three landform units is critical to
70 systematically and clearly reveal the mechanism of gully headcut erosion.

71 Previous studies suggested that gully heacut erosion is affected by various factors including

72 topography, land use change, vegetation, soil properties, and climate (Vanwallegem et al., 2003;
73 Ionita, 2006; Rodzik et al., 2009; Rieke-Zapp and Nichols, 2011; Torri and Poesen, 2014; Ionita et al.,
74 2015; Vannoppen et al., 2015; Guo et al., 2019, 2020a). In terms of topography, most of studies focused
75 on the threshold relationship ($S \leq a \cdot A^b$) to initiate gully erosion (e.g., Torri and Poesen, 2014). Several
76 experimental studies demonstrated that the upstream slope gradient and headcut height have significant
77 effects on headcut erosion (e.g., Bennett, 1999; Zhang et al., 2018). Land use change is recognized as
78 having the strongest effect on processes related to gully erosion (Poesen et al., 2003; Chaplot et al.,
79 2005; Descroix et al., 2008), and also significantly affects the activation of gully headcut erosion (e.g.,
80 Torri and Poesen, 2014). In this aspect, the vegetation coverage is a parameter that is often used to
81 clarify its effect on gully erosion (e.g., De Baets et al., 2007; Martínez-Casasnovas et al., 2009),
82 however, in fact, the vegetation effect mainly depends on the root characteristics and its distribution at
83 gully head (e.g., Vannoppen et al., 2015; Guo et al., 2019). Nevertheless, at present, the most of studies
84 on gully erosion focus on the changes in gully morphology between different periods at a watershed
85 or regional scale (Vanmaercke et al., 2016), which is why the previous studies fail to address the effects
86 of root systems on gully headcut retreat. Guo et al. (2019) concluded that the grass (*Agropyron*
87 *cristatum*) could reduce soil loss and headcut retreat distance by 45.6 - 68.5%, 66.9 - 85.4%,
88 respectively, compared with bare land, and the roots of 0 - 0.5 mm in diameter showed the greatest
89 controlling influence on headcut erosion. In terms of soil properties, lots of studies have proved the
90 significant effect of soil properties on gully headcut erosion (e.g., Nazari Samani et al., 2010), which
91 is mainly related to the change in soil erodibility induced by soil properties including soil texture, soil
92 vertical joints, soluble mineral content, soil lithology, and physicochemical properties (Sanchis et al.,
93 2008; Vanmaercke et al., 2016; Guo et al., 2020a). Rainfall, the main climate factor, is closely related
94 to runoff generation and thus be expected to affect headcut erosion. Many studies have reported that
95 the initiation of gully headcut is correlated with rainfall characteristics (e.g., summation of rainfall
96 from 24-hour rains equal to or greater than 0.5 inches) (Beer and Johnson, 1963; Vandekerckhove et
97 al., 2003; Rieke-Zapp and Nichols, 2011). However, the great difference in the threshold value relating
98 to rainfall factors was found among different areas of the world due to fully different erosion
99 environments. For example, in the northeast of China, the gully erosion is the result of soil thawing,

100 rainfall runoff and snowmelt runoff (Li et al., 2016b; Xu et al., 2019). Furthermore, at present, the
101 most of studies on gully erosion were conducted to quantify the change in gully erosion (retreat rate,
102 area and volume) at different spatial and temporal scales by using remote sensing interpretation, real-
103 time monitoring and meta-analysis based on literature data (e.g., Vanmaercke et al., 2016). However,
104 the influencing mechanism of these factors on gully headcut erosion is still unclear and need to be
105 revealed in future studies.

106 Evidently, the concentrated flow upstream gully head, mainly depended on the drainage area
107 upstream gully heads and rainfall characteristics, is the main and original drive force triggering headcut
108 erosion. The runoff firstly eroded the upstream area and then was parted into two types of flow (on-
109 wall flow and jet flow) at the brinkpoint of gully headcut (Guo et al., 2021a). Consequently, the on-
110 wall flow persistently eroded headwall soil, and the jet flow violently impacted gully bed soil and
111 formed a plunge pool (Su et al., 2015; Guo et al., 2019). Subsequently, the two types of flow merged
112 again and eroded gully bed together (Zhang et al., 2018; Shi et al., 2020a). The runoff hydraulic or jet
113 flow properties at different landform units (UA, GH and GB) are significantly different, which is an
114 important reason for the difference in erosion process among different landform units. However, the
115 temporal-spatial change in runoff and jet properties during headcut erosion is still unclear and thus
116 needs to be clarified. Furthermore, at present, some experimental studies on headcut erosion of rill,
117 ephemeral gully, gully and bank gully were conducted to investigate the runoff properties, energy
118 consumption, sediment transport process, morphology evolution and empirical model (Bennett and
119 Casali, 2001; Wells et al., 2009a, 2009b; Su et al., 2014; Xu et al., 2017a; Guo et al., 2019; Shi et al.,
120 2020a). However, relatively few knowledges were obtained to systemically reveal the hydrodynamic
121 mechanism of gully headcut erosion. Therefore, elucidating the temporal-spatial changes in runoff
122 hydraulic and soil loss and hydrodynamic mechanism of UA, GH and GB is of great importance to
123 systematically reveal the hydrodynamics mechanism of gully headcut erosion.

124 Given the above-mentioned issues, a series of simulated gully headcut erosion experiments
125 subjected to inflow scouring are conducted to (1) investigate the temporal-spatial change in runoff
126 hydraulic and jet flow properties during headcut erosion, (2) quantify the dynamic change of energy
127 consumption and soil loss and their spatial distribution, and (3) reveal the erosion hydrodynamic

128 mechanism of UA, GH and GB.

129 **2 Materials and Methods**

130 **2.1 Study area**

131 This experiment was carried out at the Xifeng Soil and Water Conservation Experimental Station
132 that is located in the Nanxiaohogou watershed, Qingyang City, Gansu Province, China. The study area
133 belongs to a semi-arid continental climate with a mean annual temperature of 9.3 °C. The mean annual
134 precipitation is 546.8 mm (1954 - 2014), of which precipitation from May to September accounts for
135 76.9% of the total precipitation (Xia et al., 2017; Guo et al., 2019). The elevation ranges from 1050 to
136 1423 m. The main landforms include gentle loess-tableland, steep hillslope and gully channel, and
137 their areas account for 57.0%, 15.7% and 27.3%, respectively. The loess-tableland is characterized by
138 low slope (1 - 5°), gentle and flat terrain and fertile soil. The main soil type is loessial soil with silt
139 loam texture. Most of hillslopes have been constructed as slope-terraces. The main gully channel is
140 usually U-shaped and the branch-gully is more actively developed and easily eroded as a V-shaped by
141 runoff from loess-tableland (Xu et al., 2019). The flat loess-tableland can accumulate the 67.4% of
142 total runoff and cause serious gully erosion that can contribute 86.3% of the total soil erosion (Guo et
143 al., 2019). The original plant species have been seriously destroyed. Since the 1970s, the “Three
144 Protection Belts” system, the “Four Eco-Economical Belts” system and the “Grain for Green” project
145 (Zhao, 1994; Fu et al., 2011) were implemented to control soil erosion. The main land use on loess-
146 tableland position has always been farmland and orchards, while the land use on hillslope is sloping
147 farmland and orchards before 1999, which have been changed into forested and grassy land due to the
148 “Grain for Green” project. The current mean annual soil erosion rate has been reduced to 4350 Mg km⁻²
149 y⁻¹ in the study watershed (Guo et al., 2019). The plants are primarily artificially planted arbors and
150 herbaceous vegetation and shrubs (Guo et al., 2021b).

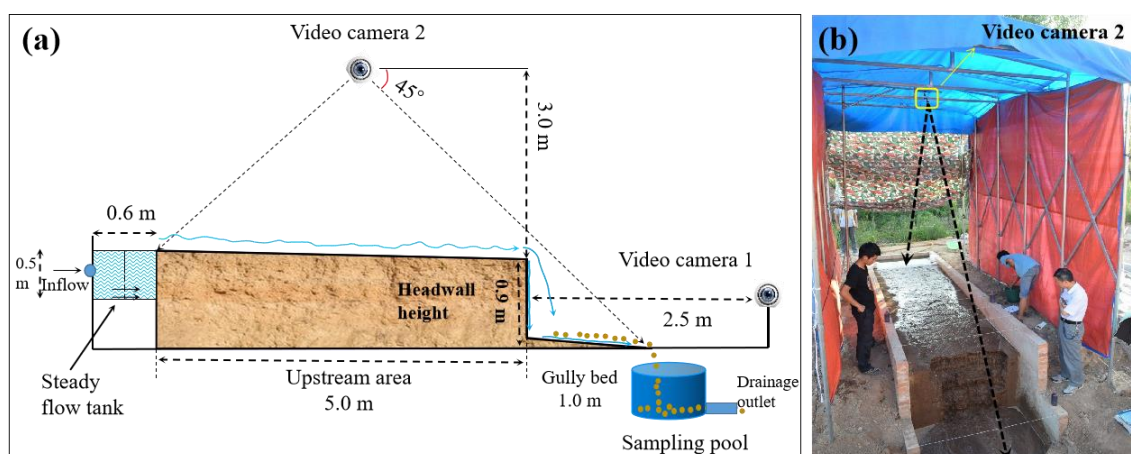
151

152 **2.2 Experimental design**

153 **2.2.1 Gully head experimental plot construction**

154 Five gully head plots for headcut erosion experiments were constructed at the experimental station
155 in April 2018. Fig. 1 shows the basic information of the gully head plot consisting of three landform

156 units (upstream area, headwall and gully bed). The plot width and slope gradient of upstream area and
 157 gully bed are uniformly designed as 1.5 m and 3°, respectively. The upstream area length, the height
 158 of the vertical headwall and the length of the gully bed are 5.0 m long, 0.9 m, and 1.0 m, respectively
 159 (Fig. 1a). The plot boundary was constructed in strict accordance with designed plot dimension using
 160 cement and bricks (Fig. 1b). After the construction of plot boundary, the soil was sieved through a 2
 161 cm sieve to remove roots and debris and ensure uniform soil underlying condition. The sieved soil was
 162 filled into the plot every 10-cm thick layer according to the investigated soil bulk density of gully
 163 heads. The soil surface of each layer was harrowed to increase the cohesion between two soil layers
 164 (Guo et al., 2019). In general, the filling upstream area length was 5.5 m that was larger than the precise
 165 upstream area length (5.0 m). After establishment of gully head plots, the five plots were carefully
 166 managed about four months (August 2018) to allow the soil to return to its nearly natural state. During
 167 the four-month conservation process, the naturally growing weeds were weeded out in time. Moreover,
 168 a flow-steady tank of 0.6 m, 1.5 m and 0.5 m in length, width and height was installed at the top of
 169 upstream area, and a circular sampling pool of 0.6 m in diameter was set at the bottom of the gully bed
 170 to collect runoff and sediment (Fig. 1a). According to the pre-experimental results, the length of
 171 upstream area can meet the needs of headcut migration under designed flow discharge ($3.0 - 7.2 \text{ m}^3 \text{ h}^{-1}$)
 172 and gully head height (0.9 m), and the length of gully bed also can satisfy the development of plunge
 173 pool by jet flow and stabilize the flow of gully bed.



174
 175 **Figure 1.** Sketch (a) and photo (b) of experimental plot

176 **2.2.2 Inflow discharge design**

177 The concentrated runoff generated from upstream area is the main force driving gully headcut

178 erosion. Jiao et al (1999) concluded that the more serious soil erosion is generally caused by “A” type
 179 rainstorm with the rainfall duration of 25 to 178 mins than other types of rainstorms in the Loess
 180 Plateau. Thus, an extreme case of rainfall duration (180 min) was considered in this study, and the
 181 recurrence period of “A” type rainstorm was designed as 30 years. Previous studies indicated that the
 182 rainstorm distribution on the Loess Plateau showed a non-significant change in past decades (Li et al.,
 183 2010; Sun et al., 2016; Wen et al., 2017). Zhang et al. (1983) proposed a statistical equation (Eq. (1))
 184 for calculating the average rainfall intensity by analyzing 1710 typical rainstorm events in the Loess
 185 Plateau. Then, the inflow discharge was calculated by Eq. (2) that involves the runoff coefficient, storm
 186 intensity and drainage area upstream gully head and ranged from 3.12 to 9.68 m³ h⁻¹. Before the study,
 187 we first conducted some preliminary experiments under some flow discharges, and meanwhile
 188 considering the pre-experiment effect, finally, we selected the five inflow discharge levels (3.0, 3.6,
 189 4.8, 6.0, and 7.2 m³ h⁻¹).

$$190 \quad RI = \frac{5.09N^{0.379}}{(t+1.4)^{0.74}} \quad (1)$$

191 where RI is the average rainfall intensity during t minutes, mm min⁻¹; N is the recurrence period
 192 of rainstorm, yr; and t is the rainfall duration, min.

$$193 \quad q = \frac{60\alpha \cdot A \cdot RI \cdot w}{W} \quad (2)$$

194 where A is the upstream area (km²) and has a wide range of 0.15 - 8.7 km² according to an early
 195 investigation of research team (Che, 2012); W is the width of the upstream area, km; w is the plot width,
 196 m; and α is the runoff coefficient of bare land and is identified as 0.167 by analyzing the runoff and
 197 rainfall data of standard runoff plots (Li et al., 2006).

198 **2.3 Experimental procedure**

199 The scouring experiment was conducted in August 2018. Before formal experiment, the upstream
 200 area length was firstly adjusted to designed length of 5.0 m (Fig. 2a). Then, a self-made tent (length ×
 201 width × height: 6.0 m × 3.0 m × 3.5 m) with waterproof canvas enclosed the plot to resist the effects
 202 of natural rainfall and sunshine on experimental progress and photo shooting for 3D reconstruction
 203 (Fig. 1b). In addition, the experimental process was recorded by two Logitech 930e video cameras
 204 with a resolution of 2.0 megapixels. The camera 1 was installed 2.5 m in front of plot headwall (Fig.
 205 1a), and the camera 2 was installed 3.0 m above the plot center (Fig. 1a).

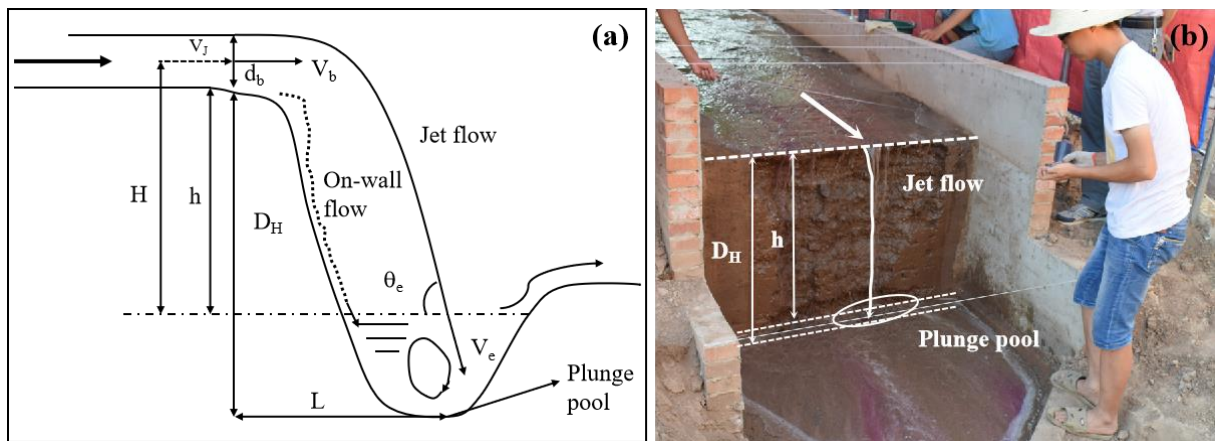
206 Before the experiment, watering can be used to spray each experimental plot until surface runoff
207 was generated, and then the plot was placed for 24 hours to ensure adequate water infiltration, which
208 can assure that the soil moisture of the five plots was approximately the same. The inlet pipeline was
209 placed in steady flow tank when the inflow discharge was adjusted to designed value. A water
210 thermometer was placed into the steady flow tank to monitor the change in water temperature during
211 experiments. The runoff and sediment samples at the plot outlet were collected at 2-min intervals to
212 represent the temporal change in runoff and sediment of “UA-GH-GB” system, and the sampling time
213 was recorded using a stopwatch (Fig. 2b). The runoff and sediment samples were oven-dried at 105 °C
214 for 24 h and weighed to calculate the soil loss rate of “UA-GH-GB” system. Besides, the timing of the
215 collapse event was recorded during headcut erosion. The upstream area was divided into 4 runoff
216 observation sections, and the runoff width (w), depth (d) and velocity (V) of each section were
217 measured by a calibrated scale of 1 mm accuracy and color tracer method (Fig. 2b, 2c). The runoff
218 velocity (V_r) before runoff arrived at the brink of headcut was measured 5 – 8 times by the flow velocity
219 measuring instrument (LS300-A). The instrument was firstly placed perpendicular to the flow section
220 but does not touch the underlying surface. When the flow passes through the turbine, the flow velocity
221 can be measured by the rotating velocity of the turbine with the accuracy of 0.01 m s^{-1} and measuring
222 error of $< 1.5\%$, and the runoff width at the headcut brinkpoint was measured (Fig. 2d). The runoff
223 width and velocity of gully bed were also measured using the same method with upstream area (Fig.
224 2e). Above mentioned measurements of runoff characteristics and sediment samples were finished in
225 2-min intervals. The whole experimental process was recorded by two video cameras and imported
226 into computers (Fig. 2f). In addition to above runoff parameters, the runoff depth (d_b) at the brink of
227 headcut, the plunge pool depth (D_H) and the vertical distance (h) from brink-point of headcut to water
228 surface of plunge pool were also measured 3 - 5 times by a steel ruler with 1 mm accuracy within each
229 2-min intervals (Fig. 3).

230



231
232
233
234
235

Figure 2. Plot construction (a), runoff width measurement of loess-tableland and runoff and sediment sampling of outlet (b), runoff velocity measurement of loess-tableland (c), jet velocity measurement of gully head (d), runoff velocity and width measurement of gully bed (e), and experimental process recoding (f)



236

Figure 3. Sketch of jet flow at gully headcut (a) and plunge pool at gully bed (b)

237
238
239
240
241
242
243
244
245

To obtain the dynamic change in morphology of erosional landform during gully headcut erosion, the experimental duration (180 min) was divided into six stages (30 - 60 - 90 - 120 - 150 - 180 min). Photo-based three-dimensional (3D) reconstruction method was employed to obtain the digital elevation model (DEM) data of each plot prior to experiment and after each 30-min test. A total of 14 target points were placed around the plot for identifying the 3D coordinate before the photos were taken. The eroded photographic was recorded by a Nikon D5300 camera with the focal length of 50 mm. The following aspects were required during photos shooting: (1) obvious water on soil surface and direct sunshine should be avoided, (2) a minimum overlap of 60% between subsequent

246 photographs was required, and (3) some complex eroded photographic should be taken in detail. In
 247 this study, the upper left corner of the plot was set as the original coordinates (0, 0, 0), and the direction
 248 of three-dimensional coordinate was determined as shown in Fig. 3d. These collected photos were
 249 imported in Agisoft PhotoScan software (Agisoft LLC, Russia, professional version 1.1.6), and then
 250 these control points and their coordinates would be identified and entered into the software. The root
 251 mean square errors for the altitudes (Z axis) of the target points are 0.0037, 0.0045, 0.0024, 0.0052 and
 252 0.0030 m on average, respectively, for the experiments of five inflow discharges, which can satisfy the
 253 study requirement (millimeter level). The DEM could be exported and was used to extract the
 254 morphological parameters and soil loss volume of three landform units at six stages (Frankl et al.,
 255 2015).

256 **2.4 Parameter calculation, data analysis and figure plotting**

257 **2.4.1 Hydraulic parameters of upstream area and gully bed**

258 Five parameters including runoff velocity (V , m s^{-1}), Reynold number (Re), Froude number (Fr),
 259 shear stress (τ , Pa) and stream power (ω , W m^{-2}) were used to characterize the changes in hydraulic
 260 properties at upstream area and gully bed positions. The several parameters except for V are calculated
 261 as follows.

$$262 \quad Re = \frac{V \cdot R}{\nu} \quad (1)$$

$$263 \quad Fr = \frac{V}{\sqrt{g \cdot R}} \quad (2)$$

$$264 \quad R = \frac{w \cdot d}{w + 2d}, \nu = \frac{1.775 \times 10^{-6}}{1 + 0.0337T + 0.000221T^2} \quad (3)$$

$$265 \quad \tau = \rho_w \cdot g \cdot R \cdot J \quad (4)$$

$$266 \quad \omega = \tau \cdot V \quad (5)$$

267 where R (m) and ν ($\text{m}^2 \text{s}^{-1}$) are the hydraulic radius and the water kinematic viscosity coefficient,
 268 respectively; w (m), d (m) and T ($^{\circ}\text{C}$) are the runoff width, depth and water temperature, respectively;
 269 ρ_w (kg m^{-3}) is the water density and J (m m^{-1}) is the hydraulic gradient.

270 **2.4.2 Jet properties of gully head**

271 Based on the measured runoff velocity (V_J , m s^{-1}) before runoff arrived at the headcut brinkpoint,
 272 the runoff depth (d_b , m) at the headcut brinkpoint, the plunge pool depth (D_H , m) and the vertical

273 distance (h , m) (Fig. 3a), the three parameters including the runoff velocity at the headcut brinkpoint
 274 (V_b), jet-flow velocity entry to plunge pool (V_e) and jet-flow shear stress (τ_j) were calculated to clarify
 275 the change of jet properties (Rouse, 1950; Hager, 1983; Stein et al., 1993; Flores-Cervantes et al., 2006;
 276 Zhang et al., 2016). The three parameters were calculated as follows.

$$277 \quad V_b = \begin{cases} \frac{\sqrt[3]{q \cdot g}}{0.715}, Fr < 1 \\ V_J \cdot \frac{Fr^2 + 0.4}{Fr^2}, Fr > 1 \end{cases} \quad (5)$$

$$278 \quad Fr = \frac{V_J}{\sqrt{g \cdot d_b}} \quad (6)$$

$$279 \quad V_e = \frac{V_b}{\cos \theta_e}, \theta_e = \arctan \left(\frac{\sqrt{2g \cdot D_H}}{V_b} \right) \quad (7)$$

$$280 \quad \tau_j = 0.025 \left(\frac{v}{q} \right)^{0.2} \cdot \rho_w \cdot [2g \cdot (h + d_b/2) + V_b^2] \quad (8)$$

281 2.4.3 Energy consumption of upstream area, gully head and gully bed

282 In this study, energy consumption of three landform units (UA, GH, GB) were calculated
 283 according to the measured runoff characteristic parameters. The bottom of GB was treated as the zero
 284 potential surface to quantify the energy consumption. Therefore, the total runoff energy (E_T , J s⁻¹), the
 285 runoff energy at the brink of headcut (E_L , J s⁻¹), the runoff energy when runoff leaves the plunge pool
 286 (E_H , J s⁻¹), and the runoff energy at the bottom of gully bed (E_B , J s⁻¹) were calculated as following.
 287 The calculation was consistent with the theory of minimum rate of energy dissipation expressed by
 288 Yang (1971a, 1971b).

$$289 \quad E_T = \rho_w g q [(L_l + L_g) \tan \theta + H_h] \quad (9)$$

$$290 \quad E_L = \rho_w g q [(L_m + L_g) \tan \theta + H_h] + \frac{1}{2} \rho_w q V_J^2 \quad (10)$$

$$291 \quad E_H = \rho_w g q \left(L_m + L_g - V_b \sqrt{\frac{2h}{g}} \right) \tan \theta + \frac{1}{2} \rho_w q V_P^2 \quad (11)$$

$$292 \quad E_B = \frac{1}{2} \rho_w q V_B^2 \quad (12)$$

293 where the L_l (m) and L_g (m) are the projection length of UA and GB, respectively, during gully
 294 head migration; L_m (m) is the gully head retreat distance; H_h (m) is the initial gully headcut height. V_P
 295 (m s⁻¹) and V_B (m s⁻¹) are the runoff velocity runoff leaving the plunge pool and GB, respectively.

296 Therefore, the total runoff energy consumption (ΔE_T , J s⁻¹), the runoff energy consumption of UA
 297 (ΔE_L , J s⁻¹), the runoff energy consumption of GH (ΔE_H , J s⁻¹) and the runoff energy consumption of

298 GB ($\Delta E_B, \text{J s}^{-1}$) could be calculated as follows.

299
$$\Delta E_T = E_T - E_B \quad (13)$$

300
$$\Delta E_L = E_T - E_L \quad (14)$$

301
$$\Delta E_H = E_L - E_H \quad (15)$$

302
$$\Delta E_B = E_H - E_B \quad (16)$$

303 **2.4.4 Statistical analysis**

304 The curve regression analysis method was employed to determine the quantitative relations
305 between hydraulic characteristics, jet properties, runoff energy consumption and soil erosion rate and
306 inflow discharge. The fitted equations between soil loss rate of three landform units and hydraulic
307 characteristics, jet properties, and energy consumption were also quantified by the curve regression.
308 The soil erosion volume of upstream area, gully head and gully bed were derived from the DEM of
309 different stages through the ArcGIS 10.0 software. The data analyse was executed by using SPSS
310 software (version 6.0) and figure plotting was carried out with Origin 8.5 and PowerPoint 2016
311 software.

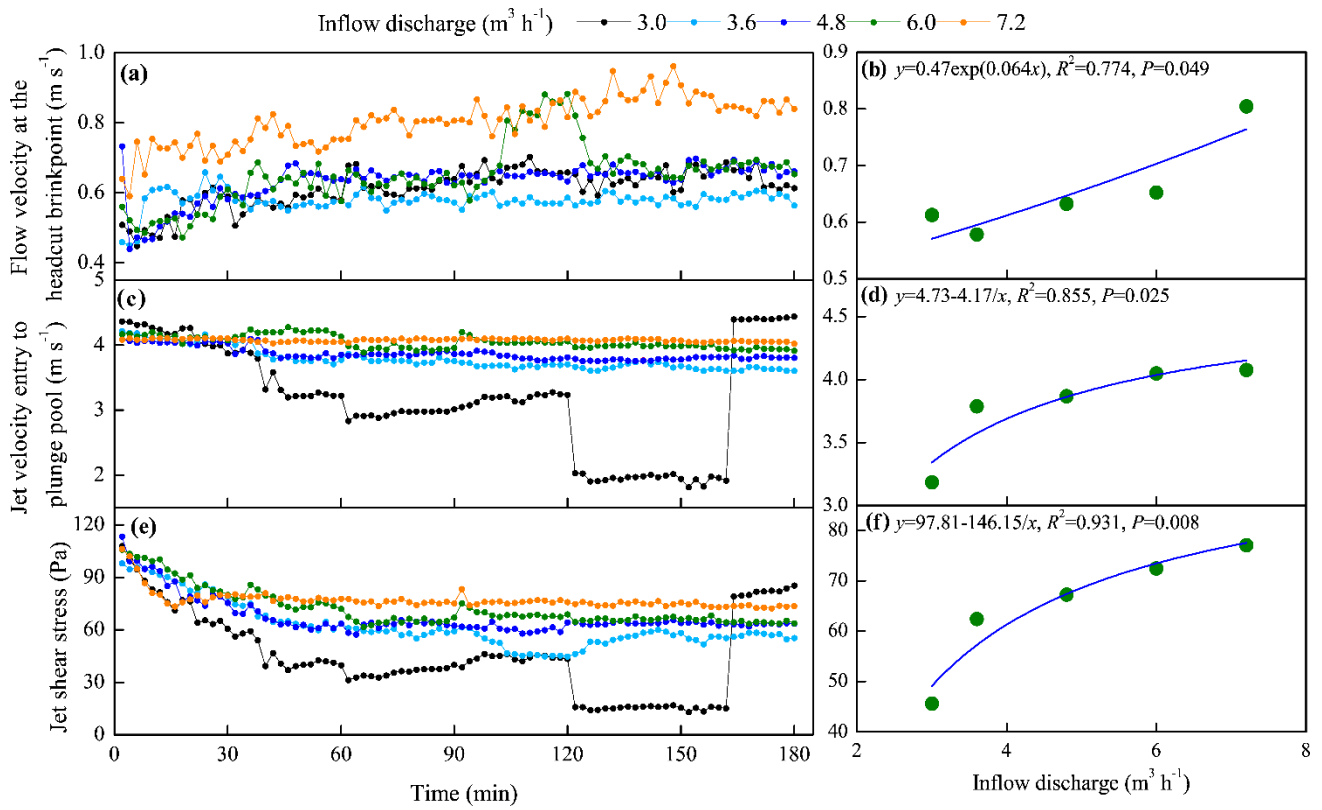
312 **3 Results**

313 **3.1 Spatial-temporal changes in jet properties and runoff hydraulic**

314 **3.1.1 Jet properties of gully head**

315 Fig. 4 shows the temporal change in the three jet property parameters of gully head (GH) under
316 different inflow discharge conditions. Overall, the flow velocity at the headcut brinkpoint (V_b)
317 increased obviously in the first 30 min and then showed a gradually stable tendency with some degree
318 of fluctuation (Fig. 4a), and the fluctuation degree was enhanced by the increased inflow discharge.
319 For example, the V_b increased sharply from 0.66 to 0.88 m s^{-1} during 100 - 124 min under 6.0 $\text{m}^3 \text{h}^{-1}$
320 inflow discharge due to the headwall failure near headcut enhancing the runoff turbulence. Regression
321 analysis revealed the significant power relationships ($V_b = a \cdot t^b$, $R^2 = 0.139 - 0.704$, $P < 0.01$) between
322 V_b and time (t) (Table 1). Furthermore, except for 3.6 $\text{m}^3 \text{h}^{-1}$ condition, the a -value increased with the
323 inflow discharge increased, but the b -value showed a weak variation (0.08 - 0.10), indicating that the
324 flow drainage from gully head can improve initial V_b but not change its change trend over time. The
325 mean V_b exhibited a significantly exponential relationship with inflow discharge (Fig. 4b, $P < 0.05$).

326 Contrary to the V_b , the jet velocity entry to plunge pool (V_e) and the jet shear stress (τ_j) experienced a
 327 gradually decreased trend with time (Fig. 4c, 4e). Notably, the V_e and τ_j suddenly decreased at 120th
 328 min and lasted nearly 40 minutes under $3.0 \text{ m}^3 \text{ h}^{-1}$ inflow discharge, which was mainly attributed to
 329 the developed second headcut shortening the jet-flow height. The temporal change of V_e could be
 330 described by logarithmic functions under $3.0 - 4.8 \text{ m}^3 \text{ h}^{-1}$ inflow discharges, and expressed by linear
 331 functions under the other inflow discharges, whereas the decrease of the τ_j with time could be presented
 332 by logarithmic functions under all inflow discharge conditions (Table 1). Furthermore, both of mean
 333 V_e and τ_j could be expressed by a positive “S” function of inflow discharge (Fig. 4d, 4f).



334

335

336

Figure 4. Temporal changes in jet properties of headcut and their relationships with inflow discharge

Table 1. The relationships between jet properties of gully headcut and time

Inflow discharge ($\text{m}^3 \text{ h}^{-1}$)	$V_b \sim t$	$V_e \sim t$	$\tau_j \sim t$
3.0	$V_b = 0.42 t^{0.09}, R^2 = 0.691$	$V_e = 5.28 - 0.49 \lg(t), R^2 = 0.290$	$\tau_j = 110.86 - 15.44 \lg(t), R^2 = 0.344$
3.6	$V_b = 0.53 t^{0.02}, R^2 = 0.139$	$V_e = 4.52 - 0.17 \lg(t), R^2 = 0.859$	$\tau_j = 117.93 - 13.14 \lg(t), R^2 = 0.823$
4.8	$V_b = 0.46 t^{0.08}, R^2 = 0.544$	$V_e = 4.25 - 0.09 \lg(t), R^2 = 0.718$	$\tau_j = 109.22 - 9.93 \lg(t), R^2 = 0.770$
6.0	$V_b = 0.52 t^{0.10}, R^2 = 0.509$	$V_e = 4.17 - 1.33 \times 10^{-3} t, R^2 = 0.478$	$\tau_j = 118.73 - 10.96 \lg(t), R^2 = 0.876$
7.2	$V_b = 0.57 t^{0.08}, R^2 = 0.704$	$V_e = 4.09 - 1.38 \times 10^{-4} t, R^2 = 0.111$	$\tau_j = 95.68 - 4.42 \lg(t), R^2 = 0.619$

337

338

Note: V_b , V_e and τ_j are runoff velocity at the headcut brinkpoint, runoff velocity entry to plunge pool and the jet shear stress, respectively. The sample number is 90 for the fitted equations, and all fitted equations are at 0.01 significant

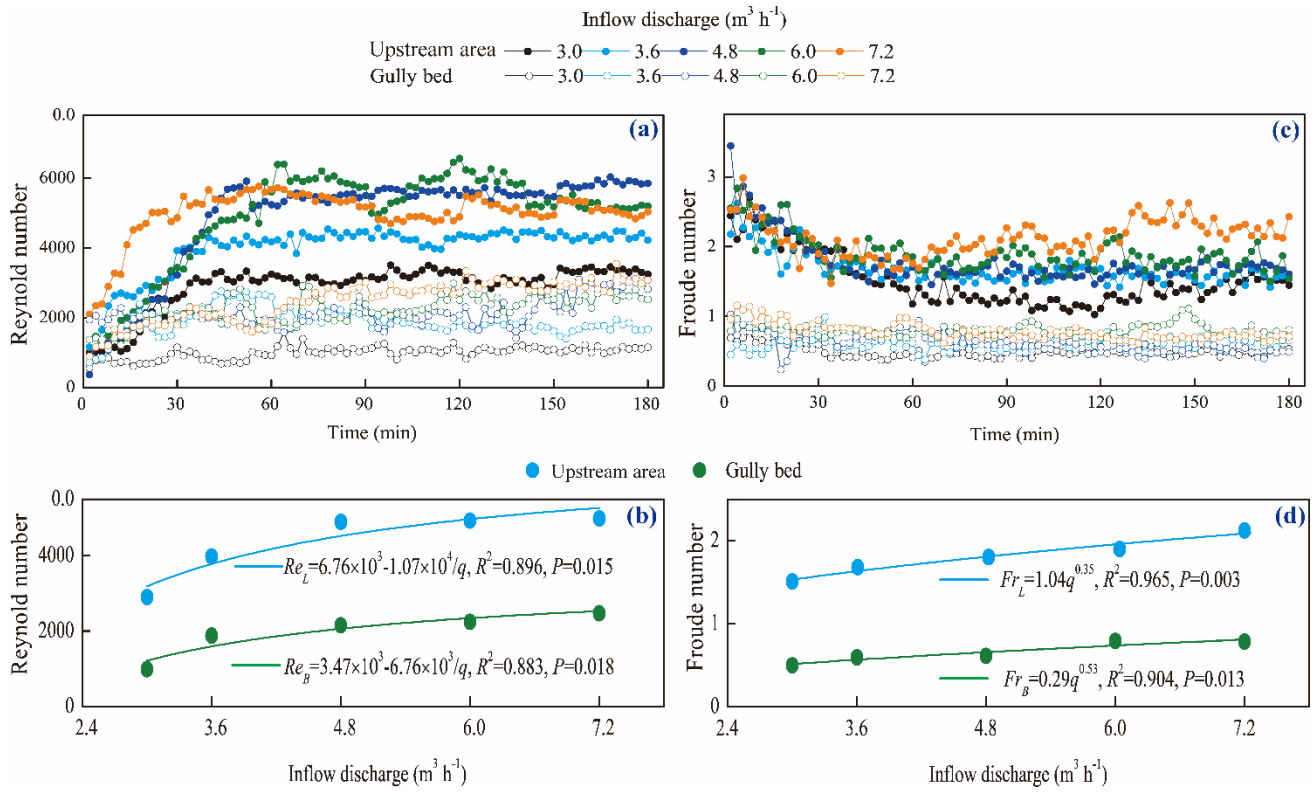
339 level.

340 **3.1.2 Runoff regime of upstream area and gully bed**

341 The temporal changes in runoff Reynold number (Re) and Froude number (Fr) of upstream area
342 (UA) and gully bed (GB) and their relationships with inflow discharge are provided in Fig. 5. The Re
343 of UA and GB showed a similar trend over time, that is, the Re firstly increased in the first 40 min and
344 then gradually stabilized (Fig. 5a). In addition, the Re of UA was larger than that of GB at any time
345 under same inflow discharge, indicating that the runoff turbulence became weaker after the runoff of
346 UA passed the gully head. The temporal variation in Re of UA could be described by logarithmic and
347 power functions, but, for the GB, the relationship was mainly dominated by power function (Table 2).
348 On average, the Re of GB was 50.5% - 65.9% less than that of UA, and the Re of UA and GB both
349 increased with the increase of inflow discharge as a power function (Fig. 5b). However, as illustrated
350 in Fig. 5c, the Fr experienced a completely opposite trend to Re . The Fr of UA decreased in the first
351 60 min and then gradually stabilized, but the Fr of GB experienced a relatively weak-fluctuating
352 variation over time. For the most of cases, the change in Fr of UA and GB over time could be expressed
353 by logarithmic functions (Table 2). On average, the Fr of UA was 2.39 - 3.04 times that of GB for
354 same inflow discharge, and the positive power function could describe the relationship between Fr and
355 inflow discharge (Fig. 5d).

356 Furthermore, the knowledge of open channel hydraulics is adopted to investigate the difference
357 in runoff regime between UA and GB. The specific definition is: the flow belongs to laminar when Re
358 is less than 500, the flow is turbulent when Re is larger than 2000, and the flow indicates transitional
359 when Re ranges from 500 to 2000; and $Fr = 1$ is the critical value for to distinguish the subcritical and
360 supercritical flow. The six flow regime zones were divided by three boundary lines ($Re = 500$, $Re =$
361 2000 , and $Fr = 1$) according to the logarithmic relationship between the flow velocity and hydraulic
362 radius (Fig. 6) (Xu et al., 2017b; Guo et al., 2020b). As shown, the runoff regimes of UA and GB were
363 located in five entirely different zones. The flow of UA was in the supercritical-transition flow regime
364 in the first 26 min and then gradually transformed to supercritical-turbulent flow regime under 3.0 -
365 $6.0 \text{ m}^3 \text{ h}^{-1}$ inflow discharge, but the flow was always in the supercritical-turbulent regime zone under
366 $7.2 \text{ m}^3 \text{ h}^{-1}$ inflow discharge. Moreover, the higher inflow discharge would enhance the flow turbulent

372 degree. The flow of GB belonged to subcritical-laminar flow category in the initial 6 min, and then
 373 transformed to subcritical-transition and subcritical-turbulent flow regime when inflow discharge was
 374 3.0 and 3.6 m³ h⁻¹. The flow was in the subcritical-turbulent flow regime in most of experimental
 375 duration when the inflow discharge was 4.8 - 7.2 m³ h⁻¹. The difference in flow regime between UA
 and GB also indicated that the presence of gully head can greatly reduce flow turbulence.



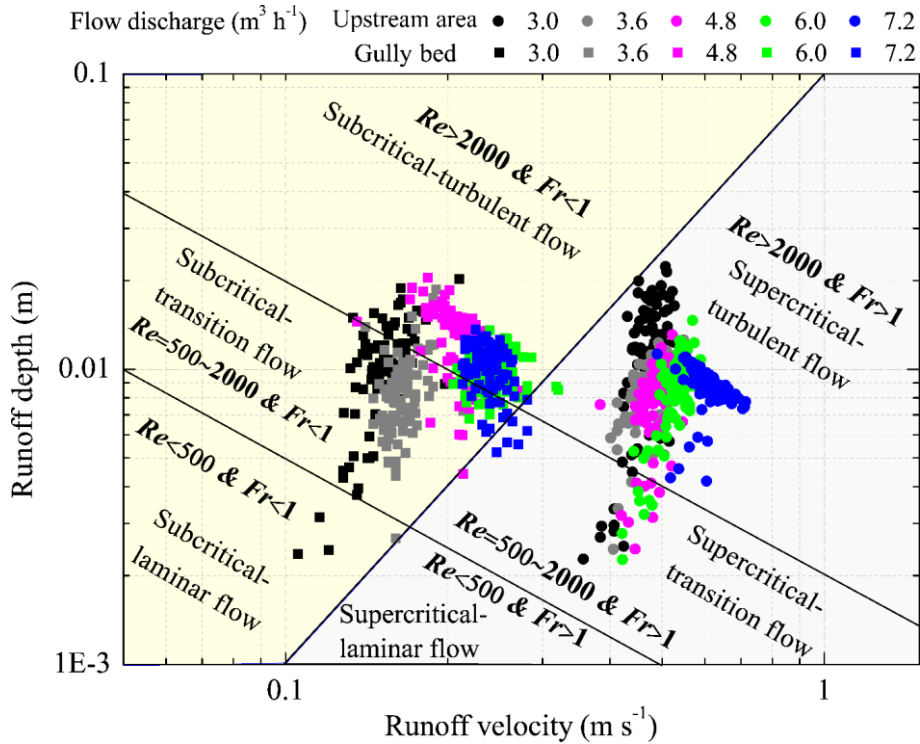
372
 373 **Figure 5.** Temporal changes in runoff regime of upstream area and gully bed and their relationships with inflow
 374 discharge
 375

Table 2. Relationships between runoff hydraulic parameters and time

Variable	Landfor m unit	Inflow discharge (m ³ h ⁻¹)				
		3.0	3.6	4.8	6.0	7.2
Reynold number	UA	$Re = 618.69 \lg(t) + 286.69, R^2 = 0.761$	$Re = 705.93 \lg(t) + 1006, R^2 = 0.815$	$Re = 1433 \lg(t) - 1159, R^2 = 0.849$	$Re = 946.64 t^{0.38}, R^2 = 0.794$	$Re = 2760 t^{0.14}, R^2 = 0.486$
	GB	$Re = 514.36 t^{0.15}, R^2 = 0.504$	—	$Re = 4.31 t + 1760, R^2 = 0.334$	$Re = 1.12 \times 10^3 t^{0.16}, R^2 = 0.566$	$Re = 744.99 t^{0.28}, R^2 = 0.872$
Froude number	UA	$Fr = 2.89 - 0.33 \lg(t), R^2 = 0.651$	$Fr = 2.46 - 0.19 \lg(t), R^2 = 0.651$	$Fr = 3.27 - 0.35 \lg(t), R^2 = 0.656$	$Fr = 2.76 - 0.20 \lg(t), R^2 = 0.515$	—
	GB	$Fr = 0.72 - 0.05 \lg(t), R^2 = 0.326$	—	$Fr = 1.0 - 0.09 \lg(t), R^2 = 0.359$	—	$Fr = 1.21 - 0.10 \lg(t), R^2 = 0.634$
Shear stress	UA	$\tau = 0.66 \lg(t) + 0.55, R^2 = 0.737$	$\tau = 1.18 \lg(t) + 0.78, R^2 = 0.813$	$\tau = 1.32 \lg(t) - 0.62, R^2 = 0.817$	$\tau = 1.50 \lg(t) - 0.63, R^2 = 0.663$	$\tau = 1.11 \lg(t) + 0.99, R^2 = 0.819$
	GB	$\tau = 2.44 t^{0.08}, R^2 = 0.205$	$\tau = 3.88 t^{0.05}, R^2 = 0.106$	$\tau = 2.27 t^{0.19}, R^2 = 0.664$	$\tau = 3.64 t^{0.12}, R^2 = 0.212$	$\tau = 1.99 t^{0.27}, R^2 = 0.686$

Stream power	UA	$\omega = 0.34 \lg(t) + 0.16, R^2 = 0.761$	$\omega = 0.38 \lg(t) + 0.55, R^2 = 0.815$	$\omega = 0.78 \lg(t) - 0.63, R^2 = 0.849$	$\omega = 0.69 \lg(t) - 0.23, R^2 = 0.737$	$\omega = 0.27 \lg(t) + 1.56, R^2 = 0.436$
	GB	$\omega = 0.28 t^{0.15}, R^2 = 0.504$	$\omega = 0.69 t^{0.09}, R^2 = 0.123$	$\omega = 0.50 t^{0.19}, R^2 = 0.540$	$\omega = 0.83 t^{0.09}, R^2 = 0.338$	$\omega = 0.51 t^{0.23}, R^2 = 0.806$

376 Note: UA and GB refer to upstream area and gully bed. Re , Fr , τ and ω are Reynold number, Froude number, shear
377 stress, stream power, respectively. The sample number is 90 for the fitted equations, and the fitted equations are at
378 0.01 significant level.

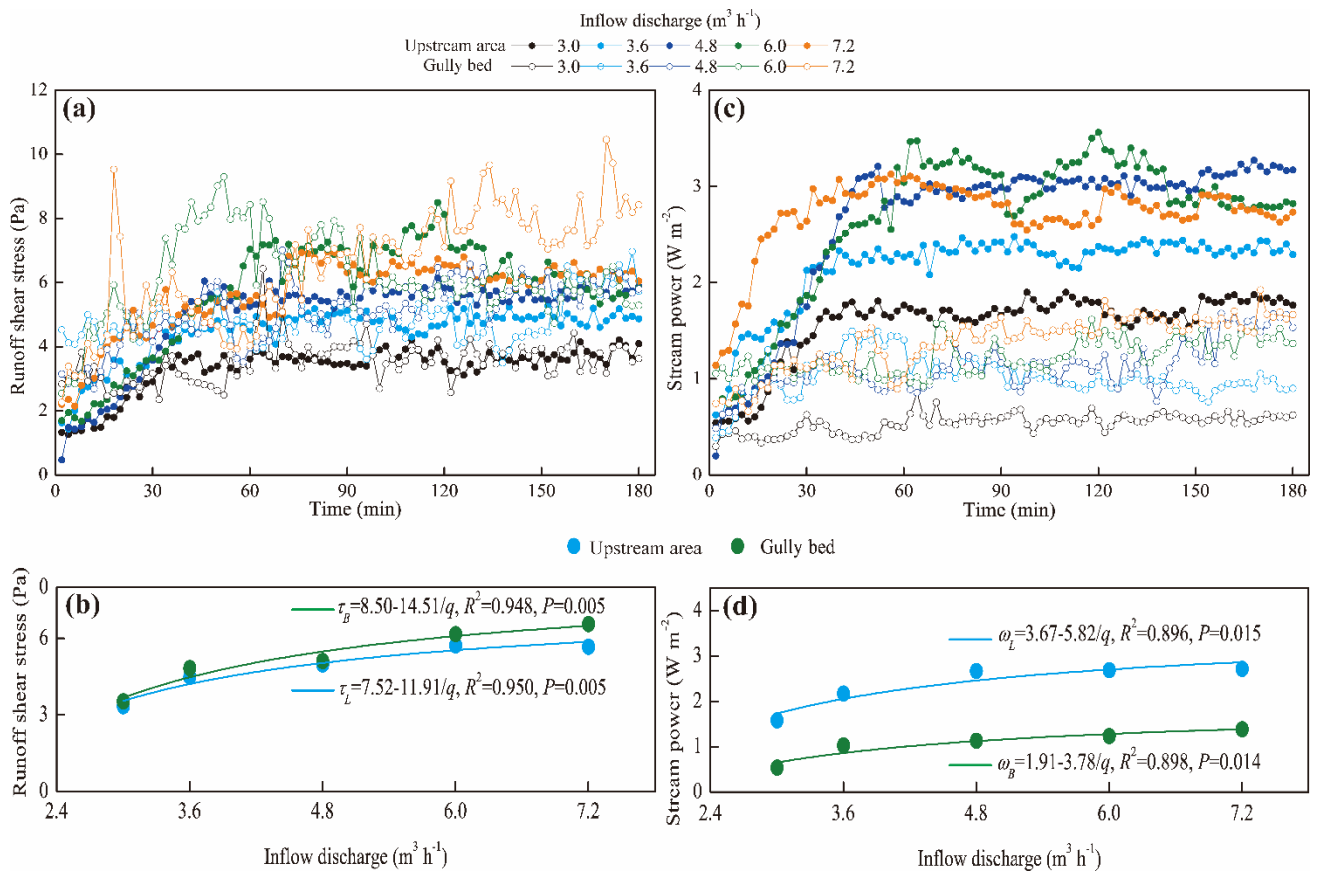


379
380 **Figure 6.** Runoff regime zones of upstream area and gully bed under different inflow discharge conditions.

381 3.1.3 Runoff shear stress and stream power of upstream area and gully bed

382 Fig.7 shows the temporal changes in runoff shear stress (τ) and stream power (ω) of upstream
383 area (UA) and gully bed (GB) and their relationships with inflow discharge. Overall, the τ of UA and
384 GB exhibited a gradually increased trend in the first 60 min, and whereafter, a relative steady state was
385 obtained, but the larger inflow discharge perturbed the steady situation (Fig. 7a). Furthermore, the
386 temporal change in τ of UA could be expressed by logarithmic functions, but the τ of GB showed a
387 significant power function with experimental time (Table 2). On average, the τ of GB was 2.8% - 15.7%
388 larger than the UA. The averaged τ of UA and GB increased with inflow discharge as a power function
389 ($\tau = a - b/q$), and the GB had a faster increased-speed (b -value) than UA (Fig. 7b), signifying that the
390 difference in τ between UA and GB would be widened with the inflow discharge increased. Similarly,
391 the ω of UA and GB also exhibited a trend of gradual increase and stabilization (Fig. 7c). Different

392 from the temporal change in τ , the ω of GB was always less than that of UA at any time for five inflow
 393 discharges. Likewise, the variation in ω of UA and GB over time exhibited a significant logarithmic
 394 and power function, respectively. On average, the ω of GB was 49.2% - 65.9% less than UA, and the
 395 positive increase in ω of UA and GB with inflow discharge could be expressed by a power function
 396 (Fig. 7d).



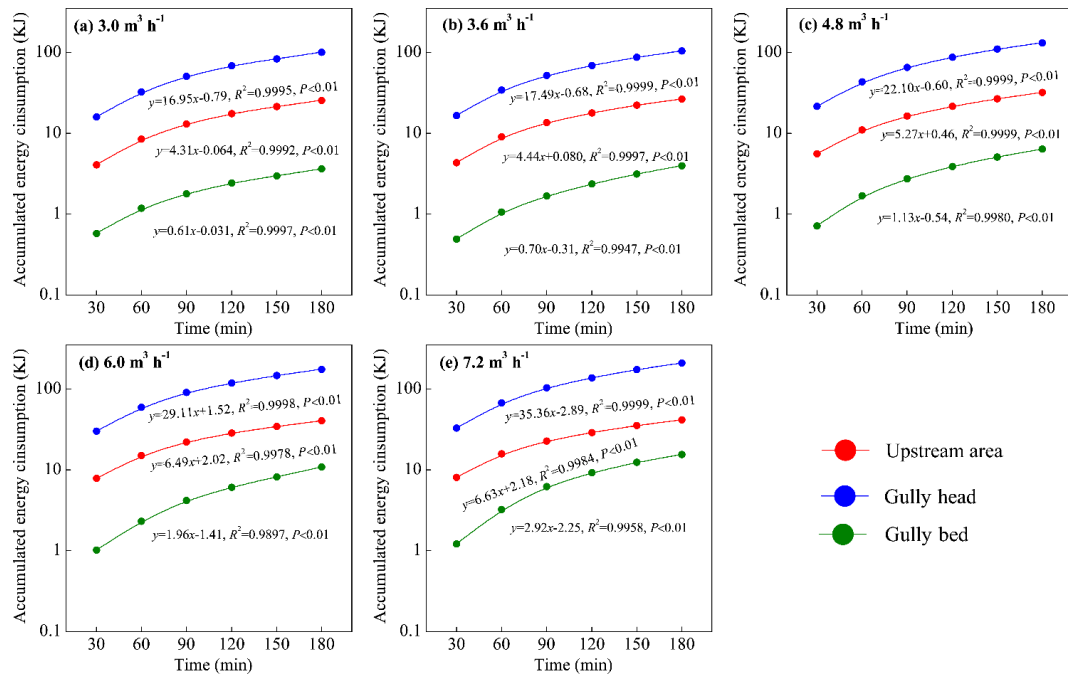
397
 398 **Figure 7.** Temporal changes in runoff shear stress and stream power of upstream area and gully bed and their
 399 relationships with inflow discharge

400 3.2 Spatial-temporal change of energy consumption

401 Fig. 8 illustrates the temporal change in accumulated energy consumption of upstream area (UA),
 402 gully head (GH) and gully bed (GB). The accumulated energy consumption of the three landform units
 403 continued to linearly increase with time ($R^2 = 0.990 - 0.999$, $P < 0.01$), of which the accumulated energy
 404 consumption in GH was always the highest at any time, followed by UA and GB under five inflow
 405 discharges. Moreover, the energy consumption rate (the slope-value of fitted equation) in the three
 406 landform units is basically constant, indicating the spatial-temporal change in energy consumption
 407 maintained a relatively steady state during gully headcut erosion. Moreover, the energy consumption

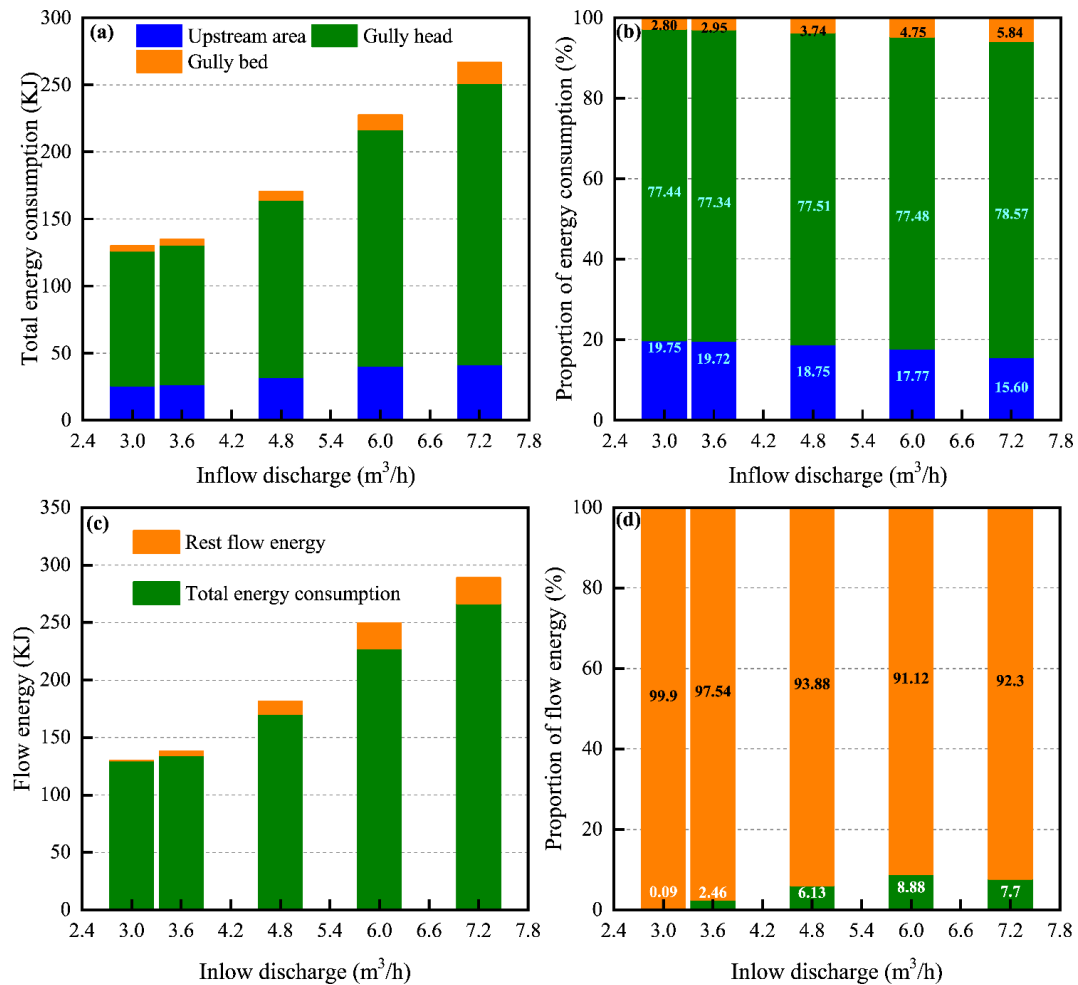
408 rate of GH was the highest, followed by UA and GB, and the energy consumption rate in the three
409 landform units also increased with the increase of inflow discharge.

410 The variations of total energy consumption of UA, GH and GB and their proportions with inflow
411 discharge are shown in Fig. 9. As illustrated in Fig. 9a, both of the total energy consumption of the
412 “UA-GH-GB” system and the three landform units increased with the increase of inflow discharge.
413 When inflow discharge increased from 3.0 to 7.2 m³ h⁻¹, the total energy consumption of the system,
414 UA, GH and GB increased by 3.6% - 105.3%, 3.4% - 62.0%, 3.5% - 108.2% and 9.0% - 327.5%,
415 respectively. Regression analysis revealed that the energy consumption of the system and the three
416 landform units increased with inflow discharge as an exponential function ($y = a \cdot \exp(b \cdot x)$, $a = 1.14 -$
417 55.41 , $b = 0.13 - 0.36$, $R^2 = 0.954 - 0.992$, $P < 0.05$). Furthermore, in view of the proportion of energy
418 consumption, the energy consumption of UA accounted for 15.6% - 19.8% of total energy consumption,
419 and linearly decreased with inflow discharge increased ($R^2 = 0.933$, $P < 0.05$), whereas the proportion
420 in GB (2.8% - 5.8%) linearly increased with inflow discharge increased ($R^2 = 0.983$, $P < 0.05$). However,
421 the proportion of energy consumption (77.3% - 78.6%) in GH showed a weak change with inflow
422 discharge (Fig. 9b), signifying that the most of runoff energy (77.5% on average) was consumed in the
423 gully head position during headcut migration. Furthermore, we found that the total energy consumption
424 (129.89 - 266.60 KJ) under different flow discharge conditions accounted for the 91.12% - 99.90% of
425 total flow energy (Fig. 9c, 9d), which also indicated that only 0.10% - 8.88% of total flow energy
426 remained at the outlet of the “UA-GH-GB” system. These results fully implied that the most of flow
427 energy (>91.12%) upstream from gully heads would be consumed during gully erosion, of which the
428 gully headcut erosion (including plunge pool erosion) is the main process consuming flow energy.



429
430
431

Figure 8. Temporal changes in runoff energy consumption of upstream area, gully head and gully bed under different inflow discharge conditions



432
433

Figure 9. Total energy consumption (a) and their proportions (b) of upstream area, gully head and gully bed, and

434 the total energy consumption and rest flow energy (c) and their proportions (d) with under different inflow
435 discharge conditions

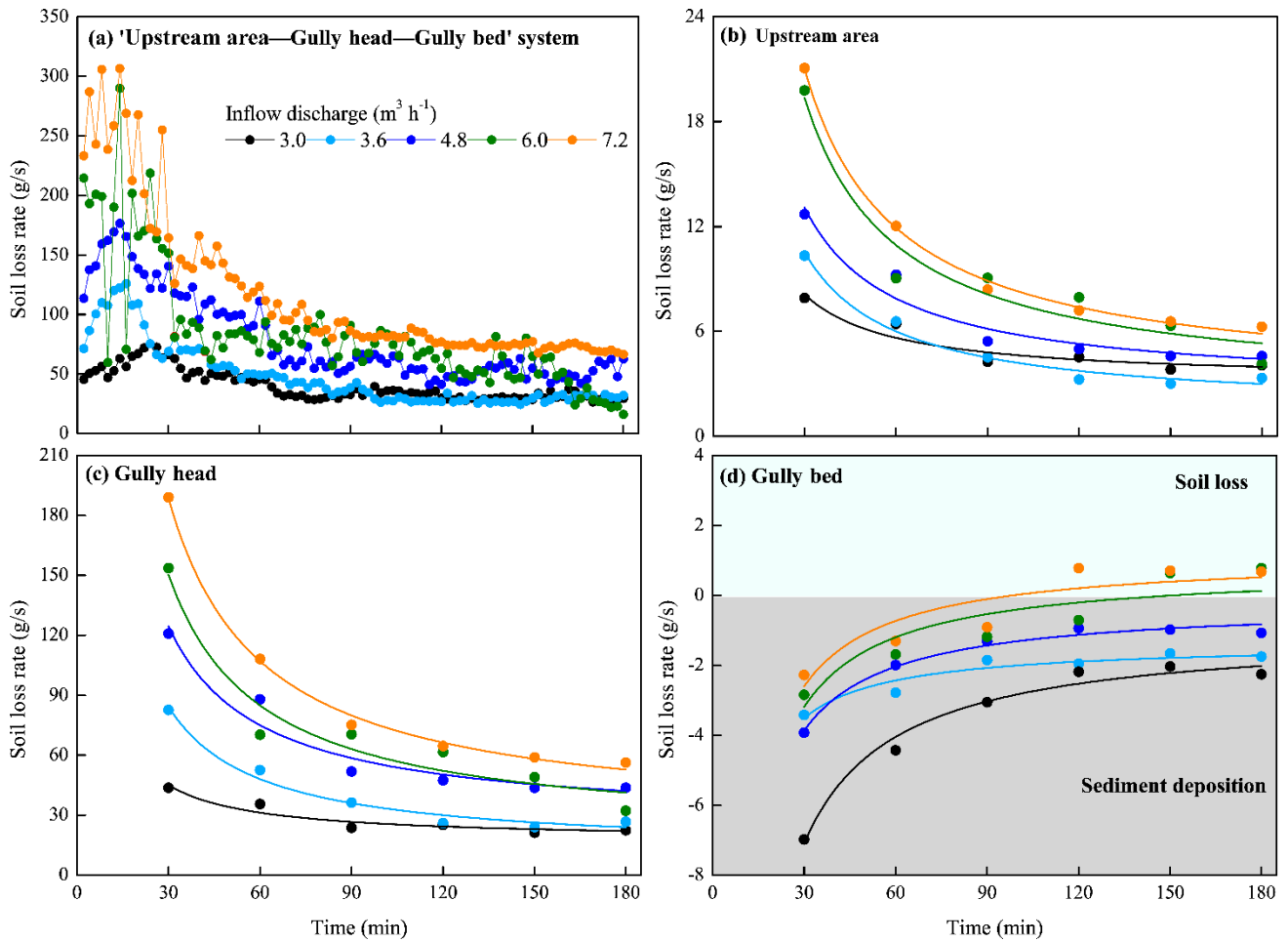
436 **3.3 Spatial-temporal change of soil loss**

437 **3.3.1 Soil loss process**

438 Fig. 10a shows that the soil loss rate of the “upstream area (UA)-gully head (GH)-gully bed (GB)”
439 system rose to a peak in first 20 min, then gradually descend and levelled off. Especially for the 6.0
440 and 7.2 m³ h⁻¹, the soil loss rate showed a severe fluctuation trend in the first 30 min. The peak soil
441 loss rate increased from 75.4 to 306.9 g s⁻¹ with increasing inflow discharge. The soil loss of UA and
442 GH experienced a similar change process. The soil loss rate was the highest in the early stage of the
443 experiment, and gradually decreased with time, and became stable after 120 min (Fig. 10b, 10c).
444 Furthermore, the temporal variation in soil loss of UA and GH could be well expressed by logarithmic
445 function ($S_L = a - b \cdot \ln(t)$, $P < 0.05$, Table 3), and the a -value (representing initial soil loss rate) and b -
446 value (reflecting the reduction rate of soil loss rate with time) increased with increasing inflow
447 discharge, indicating that larger inflow discharge can improve initial soil loss of UA and GH and also
448 expedite the decrease of soil loss rate.

449 However, the GB presented a completely different soil loss process from UA and GH (Fig. 10d).
450 The GB was always characterized by sediment deposition during the whole experiment for the 3.0 -
451 4.8 m³ h⁻¹ inflow discharges. The sediment deposition rate gradually decreased with time and presented
452 a significant “S” function over time ($S_B = a/t - b$, $R^2 = 0.918 - 0.982$, $P < 0.01$, Table 3). When the inflow
453 discharge was larger than 4.8 m³ h⁻¹, the sediment generated from UA and GH was deposited firstly in
454 the GB and then gradually transported, and the temporal change of deposited sediment on GB accorded
455 with logarithmic functions ($R^2 = 0.936$ and 0.906 , $P < 0.01$, Table 3). Furthermore, two critical time
456 points (135 min and 111 min) can be derived from the two fitted logarithmic equations, which
457 distinguished sediment deposition from sediment transport, signifying that the runoff began to
458 transport the deposited sediment on GB after 135 min and 111 min for 6.0 and 7.2 m³ h⁻¹ inflow
459 discharges.

460



461
462
463
464

Figure 10. Temporal variation in soil loss rate of the “upstream area—gully head—gully bed” system (a), upstream area (b), gully head (c) and gully bed (d)

Table 3. Relationships between soil loss rate of three landform units and time

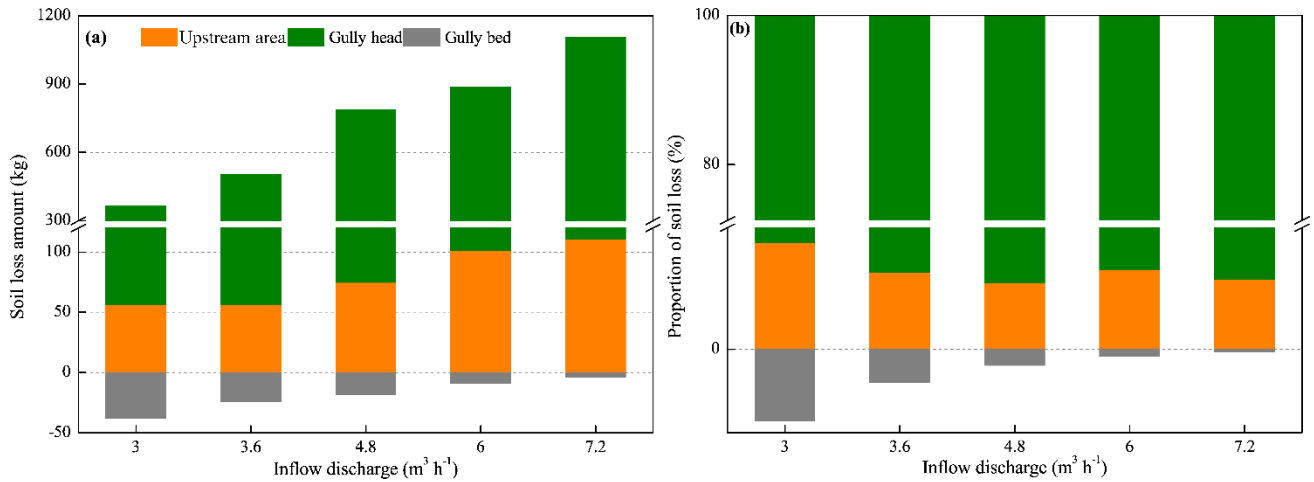
Inflow discharge ($\text{m}^3 \text{h}^{-1}$)	Fitted equations		
	Upstream area	Gully head	Gully bed
3.0	$S_L = 15.71 - 2.34 \ln(t), R^2 = 0.909^{**}$	$S_H = 87.12 - 12.99 \ln(t), R^2 = 0.908^{**}$	$S_B = -182.62/t - 1.01, R^2 = 0.980^{**}$
3.6	$S_L = 23.97 - 4.18 \ln(t), R^2 = 0.938^{**}$	$S_H = 191.82 - 33.44 \ln(t), R^2 = 0.939^{**}$	$S_B = -64.46/t - 1.36, R^2 = 0.918^{**}$
4.8	$S_L = 28.76 - 4.85 \ln(t), R^2 = 0.930^{**}$	$S_H = 273.64 - 46.17 \ln(t), R^2 = 0.929^{**}$	$S_B = -109.36/t - 0.22, R^2 = 0.982^{**}$
6.0	$S_L = 44.0 - 7.69 \ln(t), R^2 = 0.884^*$	$S_H = 341.59 - 59.74 \ln(t), R^2 = 0.885^*$	$S_B = 2.03 \ln(t) - 9.96, R^2 = 0.936^{**}$
7.2	$S_L = 47.34 - 8.25 \ln(t), R^2 = 0.922^{**}$	$S_H = 425.24 - 74.07 \ln(t), R^2 = 0.924^{**}$	$S_B = 1.86 \ln(t) - 8.76, R^2 = 0.906^{**}$

465 Note: S_L , S_H and S_B are the soil loss rate of upstream area, gully head and gully bed, respectively. The sample No. is
466 6 for fitting equation. * and ** indicate the significant level of 0.05 and 0.01.

467 3.3.2 Spatial distribution of soil loss

468 The variation in soil loss amount and proportion of the three landform units (UA, GH, GB) with
469 inflow discharge is shown in Fig. 11. As illustrated in Fig. 11a, for the experiments of five inflow
470 discharges, the soil loss was dominant in the UA and GH, but the GB was dominated by sediment

471 deposition due to the weaker sediment transport capacity of runoff on GB than sediment deliverability
 472 of UA and GH. Furthermore, the soil loss amount of UA and GH ranged from 55.9 to 110.7 kg and
 473 from 310.0 to 994.8 kg, respectively, and increased linearly with increasing inflow discharge ($R^2 =$
 474 0.966 and 0.969, $P < 0.05$). The sediment deposition amount of GB ranged from 4.2 to 37.7 kg, and
 475 decreased with inflow discharge as a logarithmic function ($R^2 = 0.961$, $P < 0.05$). In terms of proportion
 476 of soil loss (Fig. 11b), the proportion of UA and GH reached the maximum (15.3%) and minimum
 477 (84.7%), respectively under $3.0 \text{ m}^3 \text{ h}^{-1}$ inflow discharge, whereas, the proportion exhibited a little
 478 change (UA: 9.5% - 11.4%; GH: 88.6% - 90.5%) when the inflow discharge is $7.2 \text{ m}^3 \text{ h}^{-1}$. Remarkably,
 479 the proportion of deposited sediment amount on GB to total soil loss amount ranged from 0.4% to
 480 10.3%, and decreased exponentially with inflow discharge ($R^2 = 0.992$, $P < 0.001$).



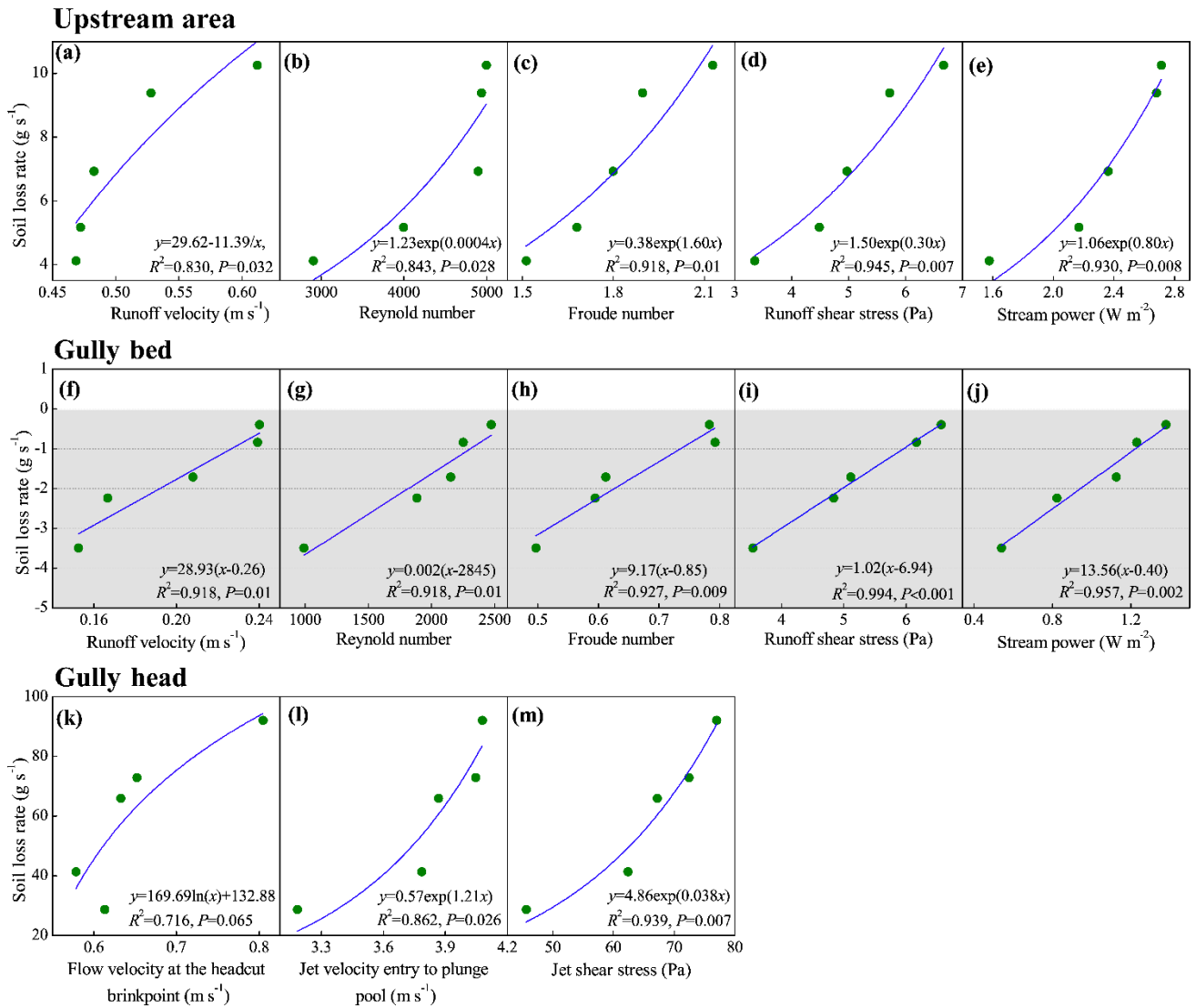
481
 482 **Figure 11.** Variation in soil loss amount (a) and proportion (b) of upstream area, gully head and gully bed with
 483 inflow discharge

484 3.4 Spatial change in hydrodynamic mechanism of soil loss

485 3.4.1 Relationships between soil loss and hydraulic parameters

486 Fig. 12 indicates the significant difference in the relationships between soil loss rate and hydraulic
 487 parameters among the three landform units (Fig. 12). For the upstream area (UA), the soil loss rate
 488 could be described as a series of exponential functions of runoff velocity, Reynold number, Froude
 489 number, runoff shear stress and stream power, of which the runoff shear stress and stream power had
 490 a closer correlation with soil loss (Fig. 12a - 12e, $R^2 = 0.830 - 0.945$). Furthermore, the increased speed
 491 of soil loss rate obviously increased with the increasing hydraulic parameters (except for runoff
 492 velocity), indicating that soil loss of UA showed a stronger sensitive response to increasing hydraulic

493 properties. However, the soil loss rate of gully bed (GB) linearly increased with the above-mentioned
 494 five parameters (Fig. 12f - 12j, $R^2 = 0.918 - 0.994$), which suggested that the decreased rate of sediment
 495 deposition of GB is basically constant with the increasing hydraulic properties. Further analysis
 496 showed that the critical runoff velocity, Reynold number, Froude number, runoff shear stress and
 497 stream power for triggering the transformation of sediment deposition to soil erosion on GB, and the
 498 critical values are 0.26 m s^{-1} , 2845, 0.85, 6.94 Pa and 0.40 W m^{-2} , respectively. For the gully head (GH)
 499 position, the soil loss was significantly affected by jet velocity entry to plunge pool and jet shear stress
 500 (Fig. 12l and 12m, $R^2 = 0.862$ and 0.939), while the relationship between soil loss and flow velocity at
 501 the headcut brink-point was not significant (Fig. 12k, $P = 0.065$).

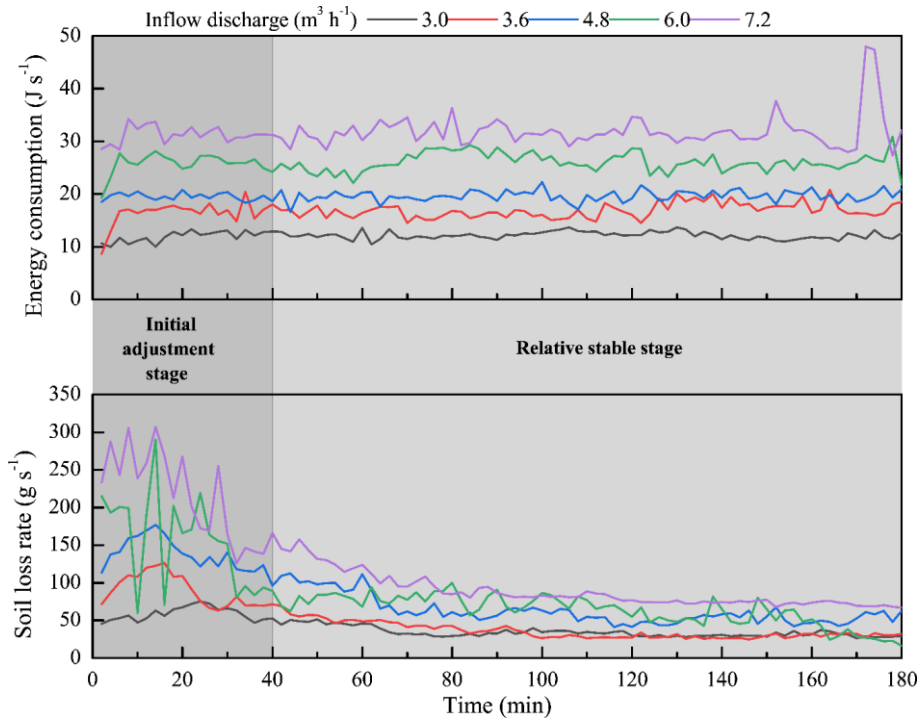


502
 503 **Figure 12.** Relationships between soil loss rate of upstream area, gully bed and gully head and runoff hydraulic and
 504 jet properties

505 3.4.2 Response of soil loss to energy consumption

506 The synchronous change of soil loss of “UA-GH-GB” system and total energy consumption can
507 be divided into two stages (Fig. 13). In the initial adjustment stage (0 - 40 min), the topsoil layer of
508 UA had the relative higher erodibility and was the main resource of soil loss, which caused the relative
509 lower flow velocity at the brinkpoint of gully head. Therefore, the most of flow discharge was
510 transformed as on-wall flow, so the most of flow energy consumed at the headwall. So, in this stage,
511 UA and gully headwall are the main positions of soil loss, and the most of flow energy was also
512 consumed in the two positions. With the gradual adjustment of upstream area morphology, the gully
513 erosion process entered into the relative stable stage (40 - 180 min). In this stage, the flow velocity at
514 headcut obviously increased and showed a slight change (Fig. 4a), and thus the headwall erosion and
515 plunge pool erosion also experienced a relative stable process. As a result, the soil loss and flow energy
516 consumption exhibited a similar change process. Occasionally, the occurrence of several gully head
517 and bank collapse events altered the synchronous change process of soil loss and energy consumption.

518 As illustrated in Fig. 14, on average, the soil loss rate of the “UA-GH-GB” system and the three
519 individual landform units was positively and significantly related to the energy consumption ($P < 0.05$),
520 and a logarithmic function was found to fit the relationship between soil loss rate and energy
521 consumption best ($R^2 = 0.889 - 0.987$). The critical energy consumption initiating the system is 7.53 J s^{-1}
522 (J s^{-1}) (Fig. 14a). Furthermore, there is critical energy consumption to initiate soil erosion of the upstream
523 area (UA) and gully head (GH) based on the fitted logarithmic functions (Fig. 14b, 14c). The critical
524 energy consumption for GH (5.79 J s^{-1}) is 2.57 times greater than that (1.62 J s^{-1}) of the UA. Similarly,
525 for the gully bed (Fig. 14d), the minimum energy consumption (1.64 J s^{-1}) is needed to trigger the
526 transformation of sediment deposition to soil loss. We found that the sum of critical energy
527 consumption initiating three landform units (9.05 J s^{-1}) was larger than the critical value initiating the
528 system, which was mainly attributed to the mass failure of gully head and bank inputting the additional
529 potential energy into the flow.

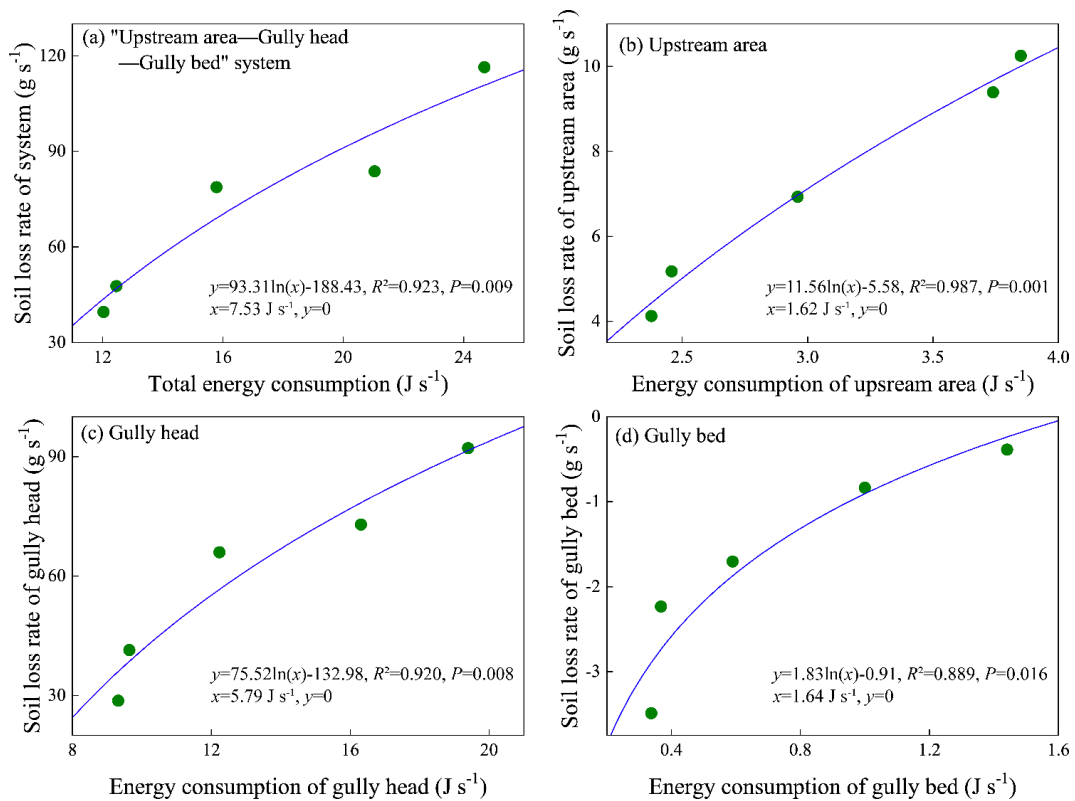


530

531

532

Figure 13. Synchronous change of soil loss rate of “upstream area-gully head-gully bed” system and total energy dissipation during headcut erosion



533

534

535

Figure 14. Relationships between soil loss rate of “upstream area-gully head-gully bed” system (a), upstream area (b), gully head (c) and gully bed(d) and energy consumption

536 4 Discussion

537 4.1 Spatial-temporal changes in hydraulic properties

538 This study showed that the runoff velocity at the headcut brink-point (V_b) firstly raised and then
539 gradually stabilized with experimental duration (Fig. 4a), which was closely corresponded to the
540 gradually decreased runoff width on the upstream area over time (Shi et al., 2020a). However, this
541 result was inconsistent with Zhang et al (2016, 2018) and Shi et al (2020b) who reported that the V_b
542 decreased over time, which was mainly due to the gradually increased roughness and resistance of
543 underlying surface over time reducing the runoff velocity in their studies (Battany and Grismer, 2015;
544 Su et al., 2015). The further analysis of power function between V_b and time ($V_b = a \cdot t^b$, Table 1) showed
545 that the a -value increased but the b -value showed a weak variation with the inflow discharge increased,
546 indicating that upstream flow discharge can improve initial V_b but not affect its change trend over time.
547 Therefore, we can extrapolate the erosion process and rule of upstream area from this simulation test
548 to the actual ground situation. By contrast, the jet velocity entry to plunge pool (V_e) and jet shear stress
549 (τ_j) experienced a gradually decreased process (Fig. 4c, 4e), which was mainly attributed to the fact
550 that the development of several second-headcut steps caused more energy consumption in plunge pools
551 and the lower potential energy at headcut brink-point due to the shortened jet flow height (Guo et al.,
552 2019; Jiang et al., 2020). This result, however, differed from the finding of Zhang et al. (2016) who
553 stated the V_e and τ_j remained stable as the experiments progressed, which was mainly attributed to the
554 weak change of jet-flow height induced by slow headcut retreat. This comparison manifested that the
555 jet flow properties was strongly determined by the headcut retreat process.

556 For the runoff hydraulic of upstream area (UA) and gully bed (GB), the Reynold number Re of
557 UA and GB initially increased and gradually stabilized, but the Froude number Fr showed an opposite
558 trend. This phenomenon was agreed with previous studies (e.g., Su et al., 2015; Zhang et al., 2016).
559 Besides, the Re and Fr of UA were larger than that of GB by 50.5% - 65.9% and 1.39 - 2.04 times,
560 respectively, under same inflow discharge upstream gully head, indicating that the runoff turbulence
561 became weaker after the runoff of UA passed the gully head and experienced plunge pool erosion (Shi
562 et al., 2020a). More evidently, the runoff on UA was in the supercritical-transition and supercritical-
563 turbulent flow regime ($Re > 500$, $Fr > 1$), whereas the runoff on GB belonged to subcritical-transition

564 and subcritical-turbulent flow regime ($Re > 500$, $Fr < 1$). However, Su et al. (2015) found that the
565 steady state Re of gully bed was higher than that of upstream area, which was mainly attributed to the
566 difference in slope gradient. In their study, the larger gully bed slope gradient than upstream area would
567 accelerate the runoff velocity and thus enhance flow turbulence (Bennett, 1999; Pan et al., 2016).
568 Furthermore, compared to UA, the τ and ω of GB increased and decreased by 2.8% - 15.7% and 49.2%
569 - 65.9%, respectively. The increased shear stress was caused by the decrease of flow velocity on gully
570 bed, and the drastically decreased stream power can reflect the energy consumption of flow for
571 transporting sediment on gully bed. This result was different from some previous experimental studies
572 on gully and bank gully under different conditions. Previous studies have proven that the lots of factors
573 including plunge pool size, slope gradient, initial step height, and soil texture influenced the hydraulic
574 properties from upstream area to gully bed is affected by various factors (Bennett and Casali, 2001;
575 Wells et al., 2009a, 2009b).

576 **4.2 Spatial-temporal change in runoff energy consumption and soil erosion**

577 Our study revealed that the accumulated runoff energy consumption of the upstream area (UA),
578 gully headcut (GH) and gully bed (GB) linearly increased over time (Fig. 8), indicating the spatial-
579 temporal change in energy consumption maintained a relatively steady state during gully headcut
580 erosion. However, the flow energy consumption of bank gully in three landform units logarithmically
581 increased over time (Su et al., 2015). This difference further manifested that the runoff energy
582 consumption of different landform units depends on gully type to some extent as well as soil texture,
583 slope and headwall height (Wells et al., 2009a). Besides, under this flow discharge conditions, the
584 proportion of energy consumption to the total flow energy ranged from 91.12% to 99.90%, indicating
585 that almost all of flow energy was consumed during headcut erosion. Furthermore, the proportion of
586 energy consumption in UA, GH and GB was 15.6% - 19.8%, 77.3% - 78.6% and 2.8% - 5.8%,
587 respectively (Fig. 9), which was also indirectly supported by the study of Su et al. (2015) who
588 suggested that the runoff energy consumption per unit soil loss from upstream area, headcut and gully
589 bed is 17.4%, 70.5% and 12.0%, respectively. This further signified that the gully head consumed the
590 most of runoff energy (77.5% on average) during headcut migration. The flow energy must be
591 consumed to surmount the soil resistance as headcut migrates, and the consumed energy was mainly

592 focused on headwall and plunge pool development (Alonso et al., 2002).

593 In terms of soil loss, our study indicated that the soil loss rate of the “UA-GH-GB” system initially
594 increased to the peak value and then gradually declined and stabilized (Fig. 10), which was consistent
595 with the results of many studies on rill and gully headcut erosion under different conditions (slope,
596 initial step height, flow discharge, soil type, soil stratification) (Bennett, 1999; Bennett and Casali,
597 2001; Gordon et al., 2007; Wells et al., 2009a; Shi et al., 2020a). Both the scour depth and sediment
598 production increased in the initial period of underlying surface adjustment, while once the plunge pool
599 development was maintained, and sediment yield decreased and gradually stabilized (Bennett et al.,
600 2000). In addition, the significant difference in soil loss process was found among the three landform
601 units. The soil loss of UA and GH decreased logarithmically over time, which was similar with several
602 studies (e.g., Su et al., 2015; Shi et al., 2020b). Nevertheless, the GB was always characterized by
603 sediment deposition for the inflow discharge of $< 4.8 \text{ m}^3 \text{ h}^{-1}$, whereas the sediment was deposited firstly
604 and then gradually transported as the inflow discharge increased to 6.0 and $7.2 \text{ m}^3 \text{ h}^{-1}$. Similar
605 phenomena were also found in some previous studies on rill headcut erosion (Bennett, 1999; Bennett
606 and Casali, 2001; Gordon et al., 2007; Wells et al., 2009a). This further indicated that soil
607 loss/deposition process of gully system was significantly influenced by three landform units, and
608 especially, the most of flow energy (77.5%) consumed at gully heads due to jet flow erosion strongly
609 weakened sediment transport capacity of flow on gully bed and thus changed the soil loss/deposition
610 process of gully system. However, Su et al. (2014, 2015) revealed a larger soil loss volume or soil loss
611 rate in gully bed than upstream area and headwall during bank gully headcut erosion. This difference
612 between our study and Su et al. (2014, 2015) is primarily caused by the difference in slope gradient.
613 The gully bed slope (20°) of bank gully was larger than that (3°) of our study, indicating the runoff on
614 gully bed of bank gully had stronger sediment transport capacity (Zhang et al., 2009; Ali et al., 2013;
615 Wu et al., 2016, 2018). Besides, some previous also proved that the soil type, surface roughness, slope-
616 length, groundwater/surface runoff were the main factors influencing soil loss by gully erosion (Amare
617 et al., 2020; Li et al., 2021). In view of the proportion of soil loss, the proportion of UA and GH was
618 9.5% - 11.4% and 88.6% - 90.5%, respectively, of which the proportion of deposited sediment on GB
619 to the sediment yield from UA and GH can reach up to 0.4% - 10.3%. This result fully demonstrated

620 that the gully head is the main source of sediment production during gully headcut erosion (Oostwoud-
621 Wijdenes & Bryan, 1994; Zhao, 1994; Su et al., 2014), and also manifested the necessary and
622 importance of gully headcut erosion controlling in gully-dominated region (Amare et al., 2019).

623 **4.3 Hydrodynamic characteristics of headcut erosion**

624 The significantly different relationships between soil loss and jet or hydraulic characteristics were
625 found among UA, GH, and GB. The soil loss rate of UA exponentially increased with five hydraulic
626 parameters (runoff velocity, Reynold number, Froude number, runoff shear stress and stream power),
627 indicating that soil loss of UA showed a stronger sensitive response to increasing hydraulic properties.
628 This could attribute to the frequent bank collapse on UA accelerating soil loss (Wells et al., 2013; Qin
629 et al., 2018). However, the sediment deposition rate of GB linearly decreased with the five hydraulic
630 parameters, signifying that sediment deposition on GB decreased at a stable state with the increase of
631 hydraulic parameters. Therefore, the sediment deposition rate would reach zero when the five
632 hydraulic parameters increased to the critical values, implying that the transformation of sediment
633 deposition to sediment transport on GB would be triggered. Furthermore, the shear stress is the optimal
634 parameter describing soil loss process of UA and GB, which differed from some studies on
635 hillslope/gully erosion hydrodynamic characteristics (Zhang et al., 2009; Shen et al., 2019; Ma et al.,
636 2020; Sidorchuk, 2020). Most of studies have verified that stream power is the superior hydrodynamic
637 parameter describing soil detachment process. This comparison also fully illustrated the great
638 difference in hydrodynamic characteristic between hillslope erosion and headcut erosion. In this study,
639 the soil loss of gully head (including plunge pool erosion) was significantly affected by jet properties.
640 It's confirmed that the plunge pool erosion by jet flow becomes a crucial process controlling gully
641 head migration and sediment production (Oostwoud-Wijdenes et al., 2000). Consequently, the plunge
642 pool erosion theory is usually employed to build several headcut retreat models (Alonso et al., 2002;
643 Campo-Bescós et al., 2013). Although the weak correlation between soil loss of gully head and flow
644 velocity at headcut breakpoint, the larger flow velocity resulted from increasing inflow discharge
645 would improve the shear stress of jet flow impinging gully bed, and thus the gully headcut suffered
646 stronger incisional erosion of the plunge pool. However, in fact, the soil loss of gully head was also
647 affected by on-wall flow erosion (Chen et al., 2013; Guo et al., 2021a), and thus more studies should

648 be conducted to clear the effect of on-wall flow properties on headwall erosion.

649 From the energy consumption perspective, the soil loss rate of the three landform units
650 significantly and logarithmically increased with the energy consumption, and the similar change trend
651 was also found in the study of Su et al. (2015). This finding suggests that energy consumption could
652 be considered as the available parameter to estimate the soil loss of gully headcut erosion (Shi et al.,
653 2020b). Furthermore, we found the critical energy consumption initiating soil erosion of UA, GH, and
654 GB are 1.62 J s^{-1} , 5.79 J s^{-1} and 1.64 J s^{-1} , respectively, indicating the soil loss of gully head (including
655 plunge pool) needs more flow energy consumption (Zhang et al., 2018; Shi et al., 2020a, 2020b). This
656 phenomenon can be attributed to the fact that the more runoff energy was consumed at the gully
657 headwall and plunge pool erosion than UA and GB and thus resulted in more severe soil loss during
658 headcut erosion. In addition, we found that the critical energy consumption activating soil loss of “UA-
659 GH-GB” system was lower the sum of critical energy consumption initiating soil loss and sediment
660 transport of three landform units (9.05 J s^{-1}). This result was closely related to mass failures such as
661 gully head and gully bank collapse can contribute the additional energy into the flow. So, the role of
662 gravitational erosion in controlling gully erosion process should be clarified in the future studies.

663 **5 Implication, significance and limitations of this study**

664 Gully erosion has been studied for nearly a century, but its process and dynamic mechanism are
665 still difficult to clearly understand and reveal. Given this, our study attempted to clarify the spatial-
666 temporal changes in flow hydraulic characteristics, energy consumption and soil loss and expound the
667 response of soil loss to runoff properties and energy consumption during headcut erosion through a
668 series of simulation experiment under controlled conditions. These results could be extended to wider
669 conditions, such as gully scale, flow discharge determined by rainfall and drainage area, which can
670 promote the understanding of process and mechanism of gully erosion under real ground conditions
671 as well as the modelling and prediction of gully erosion. Especially, the variation and proportion of
672 energy consumption along “UA-GH-GB” in the process of gully erosion and its influence on sediment
673 yield were clearly elucidated in this study, which has an important guiding significance for gully
674 erosion control practice and restoration efforts. We can design some engineering and/or vegetation
675 measures at gully heads to pre-consume the most flow energy and the energy dissipation structures

676 could be designed and installed at the position where plunge pool develops. Also, the appropriate size
677 of these measures also can be determined to ensure the flow energy of different landform units was
678 lower than the corresponding critical energy consumption.

679 However, there are some potential limitations in our study. First, considering the complex effects
680 of lots of factors on gully erosion, the flow discharge upstream gully heads was designed as the core
681 factor affecting gully erosion in our study, and the five levels of flow discharge was generated
682 according to the rainfall, landform and gully morphology. But it is not really same as the actual ground
683 situations, such as the flow discharge upstream gully heads would not be constant during a rainfall
684 event. Second, it has not been confirmed how well our experimental results are in line with the actual
685 ground results. Therefore, further studies need to verify the experimental results with the actual
686 situations, so that the study results can be practiced and applied under actual rainfall conditions. Third,
687 in the future research, gully erosion experiments under different control measures should be carried
688 out to identify suitable gully erosion prevention measures. Although the earlier-noted imperfection
689 represents the limitation of our study, we still clearly demonstrated the temporal-spatial change in
690 hydraulic properties and soil loss during headcut erosion and quantify the response relationships of
691 soil loss of different landform units to energy consumption, which is of great significance for
692 deepening the understanding of the gully process and hydrodynamic mechanism. Also, our results can
693 provide valuable ideas and scientific basis for the construction of gully erosion model and the design
694 of gully erosion prevention measures.

695 **6 Conclusions**

696 This study investigated the temporal-spatial changes in flow hydraulic, energy consumption and
697 soil loss during headcut erosion based on a series of scouring experiments of gully headcut erosion.
698 The temporal changes in jet properties of gully head (GH) were significantly affected by upstream
699 inflow discharge. The upstream area (UA) and gully bed (GB) had similar temporal changes in
700 Reynold number, Froude number, shear stress and stream power. The flow was supercritical on UA,
701 but subcritical on GB, and the turbulent degree was enhanced by the increasing inflow discharge. The
702 presence of gully headwall significantly decreased flow Reynold number, shear stress and stream
703 power, but slightly enhanced the Froude number. The accumulated energy consumption at UA, GH

704 and GB linearly increased with time. Overall, more than 91% of total flow energy was consumed
705 during headcut erosion, of which the GH accounted for 77.5% of the total runoff energy dissipation.
706 The soil loss of UA and GH decreased logarithmically over time, whereas the GB was mainly
707 characterized by sediment deposition over time. The GH and UA contributed 88.5% and 11.5% of total
708 soil loss, respectively, of which 3.8% soil loss was deposited on GB. The soil loss process of UA and
709 GH and the sediment deposition process of GB were significantly affected by flow hydraulic and jet
710 properties. Our results revealed that the critical runoff energy consumption to initiate soil erosion of
711 UA, GH and GB are 1.62 J s^{-1} , 5.79 J s^{-1} and 1.64 J s^{-1} , respectively. The runoff energy consumption
712 should be considered as a non-negligible parameter to predict gully headcut erosion.

713 **Data availability**

714 The data that support the findings of this study are available from the first author
715 (guomingming@iga.ac.cn) and corresponding author upon request (nwafu_wwl@163.com).

716 **Author contribution**

717 Mingming Guo and Wenlong Wang designed the experiments. Mingming Guo, Zhuoxin Chen,
718 Tianchao Wang, Qianhua Shi, Man Zhao and Lanqian Feng carried out the experiments. Zhuoxin Chen
719 produced and processed the digital elevation model of erosion landform. Mingming Guo and
720 Wennlong Wang written and prepared the manuscript with contributions from all co-authors.

721 **Competing interests**

722 The authors declare that they have no conflict of interest.

723 **Acknowledgments**

724 This work was supported by the National Natural Science Foundation of China (42077079,
725 41571275), the China Postdoctoral Science Foundation (2020M681062, 2021T140663), and the
726 National Key Research and Development Program of China (2016YFC0501604).

727 **References**

- 728 Addisie, M.B., Ayele, G.K., Gessess, A.A., Tilahun, S.A., Zegeye, A.D., Moges, M.M., ... Steenhuis, T.S.: Gully
729 head retreat in the sub-humid Ethiopian Highlands: The Ene-Chilala catchment, *Land Degradation &*
730 *Development*, 28, 1579–1588, <https://doi.org/10.1002/ldr.2688>, 2017.
- 731 Ali, M., Seeger, M., Sterk, G., Moore, D.: A unit stream power based sediment transport function for overland
732 flow. *Catena*. 101, 197-204. <https://doi.org/10.1016/j.catena.2012.09.006>
- 733 Alonso, C.V., Bennett, S.J., Stein, O.R., 2002. Predicting head cut erosion and migration in concentrated flows
734 typical of upland areas, *Water Resources Research*, 38, 39-1–39-15, <http://dx.doi.org/10.1029/2001WR001173>,
735 2013.
- 736 Amare, S., Keesstra, S., van der Ploeg, M., Langendoen, E., Steenhuis, T., Tilahun, S.: Causes and controlling
737 factors of Valley bottom Gullies. *Land*, 8(9), 141, <https://doi.org/10.3390/land8090141>, 2019.
- 738 Amare, S., Langendoen, E., Keesstra, S., Ploeg, M. V. D., Gelagay, H., Lemma, H., van der Zee, S. E.:
739 Susceptibility to Gully Erosion: Applying Random Forest (RF) and Frequency Ratio (FR) Approaches to a Small
740 Catchment in Ethiopia. *Water*, 13(2), 216, <https://doi.org/10.3390/w13020216>, 2021.
- 741 Arabameri, A., Chen, W., Lombardo, L., Blaschke, T., Tien Bui, D.: Hybrid computational intelligence models
742 for improvement gully erosion assessment, *Remote Sensing*, 12(12), <https://doi.org/10.3390/rs12010140>, 140,
743 2020.
- 744 Battany, M.C., Grismer, M.E.: Rainfall runoff and erosion in Napa Valley vineyards: effects of slope, cover and
745 surface roughness, *Hydrological Processes*, 14(7), 1289-1304, [https://doi.org/10.1002/\(SICI\)1099-1085\(200005\)14:7<1289::AID-HYP43>3.0.CO;2-R](https://doi.org/10.1002/(SICI)1099-1085(200005)14:7<1289::AID-HYP43>3.0.CO;2-R), 2015.
- 747 Beer, C.E., Johnson, H.P.: Factors in gully growth in the deep loess area of western Iowa. *Transactions of ASAE*,
748 6, 237–240, <https://doi.org/10.13031/2013.40877>, 1963.
- 749 Belayneh, M., Yirgu, T., Tsegaye, D.: Current extent, temporal trends, and rates of gully erosion in the Gumara
750 watershed, northwestern Ethiopia, *Global Ecology and Conservation*, 24, e01255,
751 <https://doi.org/10.1016/j.gecco.2020.e01255>, 2020.
- 752 Bennett, S.J., Casali, J.: Effect of initial step height on headcut development in upland concentrated flows. *Water*
753 *Resources Research*, 37, 1475–1484, <https://doi.org/10.1029/2000WR900373>, 2001.
- 754 Bennett, S.J.: Effect of slope on the growth and migration of headcuts in rills, *Geomorphology*, 30, 273–290,
755 [https://doi.org/10.1016/S0169-555X\(99\)00035-5](https://doi.org/10.1016/S0169-555X(99)00035-5), 1999.
- 756 Bennett, S.J., Alonso, C.V.: Turbulent flow and bed pressure within headcut scour holes due to plane reattached
757 jets, *Journal of Hydraulic Research*, 44, 510–521, <https://doi.org/10.1080/00221686.2006.9521702>, 2006.
- 758 Bennett, S.J., Alonso, C.V., Prasad, S.N., Romkens, M.J.: Experiments on headcut growth and migration in
759 concentrated flows typical of upland areas, *Water Resources Research*, 36, 1911–1922,
760 <https://doi.org/10.1029/2000WR900067>, 2000.
- 761 Bogale, A. G., Aynalem, D. W., Adem, A. A., Mekuria, W., Tilahun, S.: Spatial and temporal variability of soil
762 loss in gully erosion in upper Blue Nile basin, Ethiopia, *Applied Water Science*, 10(5), 106,
763 <https://doi.org/10.1007/s13201-020-01193-4>, 2020.
- 764 Campo-Bescós, M.A., Flores-Cervantes, J.H., Bras, R.L., Casali, J., Giráldez, J.V.: Evaluation of a gully headcut
765 retreat model using multitemporal aerial photographs and digital elevation models, *Journal of Geophysical*
766 *Research: Earth Surface*, 118, 2159–2173, <https://doi.org/10.1002/jgrf.20147>, 2013.

767 Chaplot, V., Giboire, G., Marchand, P., Valentin, C.: Dynamic modelling for linear erosion initiation and
768 development under climate and land-use changes in northern Laos, *Catena*, 63, 318–328,
769 <https://doi.org/10.1016/j.catena.2005.06.008>, 2005.

770 Che, X.L.: Study of distribution characteristic and evolution of headward erosion on Dongzhi tableland of the
771 loess gully region, Yangling: Northwest A&F University, pp. 66-67, (In Chinese), 2012.

772 Chen, A., Zhang, D., Peng, H., Fan, J., Xiong, D., Liu, G.: Experimental study on the development of collapse
773 of overhanging layers of gully in Yuanmou Valley, China, *Catena*, 109, 177-185,
774 <https://doi.org/10.1016/j.catena.2013.04.002>, 2013.

775 De Baets, S., Poesen, J., Knapen, A., Galindo, P.: Impact of root architecture on the erosion-reducing potential
776 of roots during concentrated flow, *Earth Surface Processes and Landforms*, 32, 1323–1345,
777 <https://doi.org/10.1002/esp.1470>, 2007.

778 de Vente, J., Poesen, J.: Predicting soil erosion and sediment yield at the basin scale: Scale issues and semi-
779 quantitative models, *Earth-Science Reviews*, 71, 95–125, <https://doi.org/10.1016/j.earscirev.2005.02.002>, 2005.

780 DeLong, S.B., Johnson, J., Whipple, K.: Arroyo channel head evolution in a flash-flood-dominated
781 discontinuous ephemeral stream system, *Geological Society of America Bulletin*, 126, 1683–1701,
782 <https://doi.org/10.1130/B31064.1>, 2014.

783 Descroix, L., González Barrios, J.L., Viramontes, D., Poulénard, J., Anaya, E., Esteves, M., Estrada, J.: Gully
784 and sheet erosion on subtropical mountain slopes: their respective roles and the scale effect, *Catena*, 72, 325–
785 339, <https://doi.org/10.1016/j.catena.2007.07.003>, 2008.

786 Dotterweich, M., Rodzik, J., Zglobicki, W., Schmitt, A., Schmidtchen, G., Bork, H.R.: High resolution gully
787 erosion and sedimentation processes, and land use changes since the Bronze Age and future trajectories in the
788 Kazimierz Dolny area (Nałęczów Plateau, SE-Poland), *Catena*, 95, 50–62,
789 <https://doi.org/10.1016/j.catena.2012.03.001>, 2012.

790 Flores-Cervantes, J., Istanbuluoglu, E., Bras, R.: Development of gullies on the landscape: A model of headcut
791 retreat resuUAing from plunge pool erosion, *Journal of Geophysical Research*, 111, 1–14,
792 <https://doi.org/10.1029/2004JF000226>, 2006.

793 Frankl, A., Stal, C., Abraha, A., Nyssen, J., Rieke-Zapp, D., DeWulf, A., Poesen, J.: Detailed recording of gully
794 morphology in 3D through image-based modelling, *Catena*, 127, 92–101,
795 <https://doi.org/10.1016/j.catena.2014.12.016>, 2015.

796 Fu, B.J., Liu, Y., Lv, Y.H., He, C.S., Zeng, Y., Wu, B.F.: Assessing the soil erosion control service of ecosystems
797 change in the Loess Plateau of China, *Ecological Complexity*, 8, 284-293,
798 <https://doi.org/10.1016/j.ecocom.2011.07.003>, 2011.

799 Gordon, L.M., Bennett, S.J., Wells, R.R., Alonso, C.V.: Effect of soil stratification on the development and
800 migration of headcuts in upland concentrated flows, *Water Resources Research*, 43, W07412,
801 <https://doi.org/10.1029/2006WR005659>, 2007.

802 Guo, M., Wang, W., Shi, Q., Chen, T., Kang, H., Li, J.: An experimental study on the effects of grass root density
803 on gully headcut erosion in the gully region of China's Loess Plateau, *Land Degradation & Development*, 30,
804 2107–2125, <https://doi.org/10.1002/ldr.3404>, 2019.

805 Guo, M., Wang, W., Wang, T., Wang, W., Kang, H.: Impacts of different vegetation restoration options on gully
806 head soil resistance and soil erosion in loess tablelands, *Earth Surface Processes and Landforms*, 45(4), 1038-
807 1050, <https://doi.org/10.1002/esp.4798>, 2020a.

808 Guo, M.M., Wang, W.L., Kang, H.L., Yang, B.: Changes in soil properties and erodibility of gully heads induced
809 by vegetation restoration on the Loess Plateau, China, *Journal of Arid Land*, 10(5), 712-725,
810 <https://doi.org/10.1007/s40333-018-0121-z>, 2018.

811 Guo, M.M., Wang, W.L., Li, J.M., Bai, Y., Kang, H.L., Yang, B.: Runoff characteristics and soil erosion dynamic
812 processes on four typical engineered landforms of coalfields: An in-situ simulated rainfall experimental study,
813 *Geomorphology*, 349, 106896, <https://doi.org/10.1016/j.geomorph.2019.106896>, 2020b.

814 Guo, M.M., Lou, Y.B., Chen, Z.X., Wang, W.L., Feng, L.Q., Zhang, X.Y.: The proportion of jet flow and on-
815 wall flow and its effects on soil loss and plunge pool morphology during gully headcut erosion, *Journal of*
816 *Hydrology*, 598, 126220, <https://doi.org/10.1016/j.jhydrol.2021.126220>, 2021a.

817 Guo, M.M., Chen, Z.X., Wang, W.L., Wang, T.C., Wang, W.X., Cui, Z.Q.: Revegetation induced change in soil
818 erodibility as influenced by slope situation on the Loess Plateau, *Science of the Total Environment*, 772, 145540,
819 <https://doi.org/10.1016/j.scitotenv.2021.145540>, 2021b.

820 Hager, W.H.: Hydraulics of plane free overfall, *Journal of Hydraulic Engineering*, 109, 1683–1697,
821 [https://doi.org/10.1061/\(ASCE\)0733-9429\(1983\)109:12\(1683\)](https://doi.org/10.1061/(ASCE)0733-9429(1983)109:12(1683)), 1983.

822 Hanson, G.J., Robinson, K.M., Cook, K.R.: Prediction of headcut migration using a deterministic approach,
823 *Transactions of the ASAE*, 44(4), 525-531, <https://doi.org/10.13031/2013.6112>, 2001.

824 Hosseinalizadeh, M., Kariminejad, N., Chen, W., Pourghasemi, H.R., Alinejad, M., Behbahani, A.M.,
825 Tiefenbacher, J.P.: Gully headcut susceptibility modeling using functional trees, naïve Bayes tree, and random
826 forest models, *Geoderma*, 342, 1-11, <https://doi.org/10.1016/j.geoderma.2019.01.050>, 2019.

827 Ionita, I.: Gully development in the Moldavian Plateau of Romania, *Catena*, 68, 133–140,
828 <https://doi.org/10.1016/j.catena.2006.04.008>, 2006.

829 Ionita, I., Niacsu, L., Petrovici, G., Blebea-Apostu, A.M.: Gully development in eastern Romania: a case study
830 from Falciu Hills, *Natural Hazards*, 79, 113–138, <https://doi.org/10.1007/s11069-015-1732-8>, 2015.

831 Jiang, Y., Shi, H., Wen, Z., Guo, M., Zhao, J., Cao, X., Fan, Y., Zheng, C.: The dynamic process of slope rill
832 erosion analyzed with a digital close range photogrammetry observation system under laboratory conditions,
833 *Geomorphology*, 350, 106893, <https://doi.org/10.1016/j.geomorph.2019.106893>, 2020.

834 Jiao, J.Y., Wang, W.Z., Hao, X.P.: Precipitation and erosion characteristics of rainstorm in different pattern on
835 Loess Plateau, *Journal of Arid Land Resources and Environment*, 13(1), 34-42, (In Chinese), 1999.

836 Kirkby, M.J., Bull, L.J., Poesen, J., Nachtergaele, J., Vandekerckhove, L.: Observed and modelled distributions
837 of channel and gully heads—with examples from SE Spain and Belgium, *Catena*, 50, 415–434,
838 [https://doi.org/10.1016/S0341-8162\(02\)00128-5](https://doi.org/10.1016/S0341-8162(02)00128-5), 2003.

839 Li, Binbing., Huang, Lei., Feng, Lin., Li, Peng., Yao, Jingwei., Liu, Fangming., Li, Junli., Tang, Hui.: Gully
840 sidewall expansion process on loess hill slope erosion, *Journal of Basic Science and Engineering*, 24(6), 1147-
841 1158. (In Chinese), 2016.

842 Li, H., Cruse, R.M., Liu, X.B., Zhang, X.Y.: Effects of topography and land use change on gully development
843 in typical Mollisol region of Northeast China, *Chinese Geographical Science*, 26, 779-788,
844 <https://doi.org/10.1007/s11769-016-0837-7>, 2016.

845 Li, M., Song, X.Y., Shen, B., Li, H.Y., Meng, C.X.: Influence of vegetation change on producing runoff and
846 sediment in gully region of Loess Plateau, *Journal of Northwest Sci-Tech University of AgricuUAure and*
847 *Forestry (Natural Science Edition)*, 34, 117-120, (In Chinese), 2006.

848 Li, Y., Mo, Y. Q., Are, K. S., Huang, Z., Guo, H., Tang, C., Abegunrin, T.P., Qin, Z.H, Kang, Z.W., Wang, X.:
849 Sugarcane planting patterns control ephemeral gully erosion and associated nutrient losses: Evidence from

850 hillslope observation. *Agriculture, Ecosystems & Environment*, 309, 107289,
851 <https://doi.org/10.1016/j.agee.2020.107289>, 2021.

852 Li, Z., Zhang, Y., Zhu, Q., He, Y., Yao, W.: Assessment of bank gully development and vegetation coverage on
853 the Chinese Loess Plateau, *Geomorphology*, 228, 462–469, <https://doi.org/10.1016/j.geomorph.2014.10.005>,
854 2015.

855 Li, Z., Zheng, F.L., Liu, W.Z., Flanagan, D.C.: Spatial distribution and temporal trends of extreme temperature
856 and precipitation events on the Loess Plateau of China during 1961–2007, *Quaternary International*, 226(1-2),
857 92-100, <https://doi.org/10.1016/j.quaint.2010.03.003>, 2010.

858 Ma, Q., Zhang, K., Cao, Z., Wei, M., & Yang, Z.: Soil detachment by overland flow on steep cropland in the
859 subtropical region of China, *Hydrological Processes*, 34(8), 1810-1820, <https://doi.org/10.1002/hyp.13694>,
860 2020

861 Martínez-Casasnovas, J.A., Concepción Ramos, M., García-Hernández, David.: Effects of land - use changes
862 in vegetation cover and sidewall erosion in a gully head of the Penedès region (northeast Spain), *Earth Surface*
863 *Processes & Landforms*, 34, 1927-1937, <https://doi.org/10.1002/esp.1870>, 2009.

864 Nazari Samani, A., Ahmadi, H., Mohammadi, A., Ghoddousi, J., Salajegheh, A., Boggs, G., Pishyar, R.: Factors
865 Controlling Gully Advancement and Models Evaluation (Hableh Rood Basin, Iran), *Water Resources*
866 *Management*, 24, 1532–1549, <https://doi.org/10.1007/s11269-009-9512-4>, 2010.

867 Oostwoud-Wijdenes, D., Bryan, R.B.: The significance of gully headcuts as a source of sediment on low-angle
868 slopes at Baringo, Kenya, and initial control measures, *Advances in Geocology*, 27, 205–231, 1994.

869 Oostwoud-Wijdenes, D., Poesen, J., Vandekerckhove, L., Ghesquiere, M.: Spatial distribution of gully head
870 activity and sediment supply along an ephemeral channel in a Mediterranean environment, *Catena*, 39, 147–
871 167, [http://202.194.143.28:80/rwt/SD/https/MSYXTLUQPJUB/10.1016/S0341-8162\(99\)00092-2](http://202.194.143.28:80/rwt/SD/https/MSYXTLUQPJUB/10.1016/S0341-8162(99)00092-2), 2000.

872 Pan, C., Ma, L., Wainwright, J., Shanguan, Z.: Overland flow resistances on varying slope gradients and
873 partitioning on grassed slopes under simulated rainfall, *Water Resources Research*, 52, 2490–2512,
874 <https://doi.org/10.1002/2015WR018035>, 2016.

875 Poesen, J., Nachtergaele, J., Verstraeten, G., Valentin, C.: Gully erosion and environmental change: Importance
876 and research needs, *Catena*, 50, 91-133, [https://doi.org/10.1016/S0341-8162\(02\)00143-1](https://doi.org/10.1016/S0341-8162(02)00143-1), 2003.

877 Qin, Chao., Zheng, Fenli., Wells Robert, R., Xu, Ximeng, Wang, Bin., Zhong, Keyuan.: A laboratory study of
878 channel sidewall expansion in upland concentrated flows, *Soil and Tillage Research*, 178, 22-31,
879 <https://doi.org/10.1016/j.still.2017.12.008>, 2018.

880 Reuter, H.I., Nelson, A., Jarvis, A.: An evaluation of void filling interpolation methods for SRTM data,
881 *International Journal of Geographic Information Science*, 21(9), 983-1008, 2007.

882 Rieke-Zapp, D.H., Nichols, M.H.: Headcut retreat in a semiarid watershed in the southwestern United States
883 since 1935, *Catena*, 87, 1–10, <https://doi.org/10.1016/j.catena.2011.04.002>, 2011.

884 Rodzik, J., Furtak, T., Zglobicki, W.: The impact of snowmelt and heavy rainfall runoff on erosion rates in a
885 gully system, Lublin Upland, Poland, *Earth Surface Processes & Landforms*, 34, 1938–1950,
886 <https://doi.org/10.1002/esp.1882>, 2009.

887 Rouse, H.: *Engineering hydraulics*. Hoboken, NJ: Wiley, 1950.

888 Sanchis, M.P., Torri, D., Borselli, L., Poesen, J.: Climate effects on soil erodibility, *Earth Surface Processes &*
889 *Landforms*, 33, 1082–1097, <https://doi.org/10.1002/esp.1604>, 2008.

890 Shen, N., Wang, Z., Zhang, Q., Chen, H., Wu, B.: Modelling soil detachment capacity by rill flow with hydraulic
891 variables on a simulated steep loessial hillslope, *Hydrology Research*, 50(1), 85-98,
892 <https://doi.org/10.2166/nh.2018.037>, 2018.

893 Shi, Q.H., Wang, W.L., Guo, M.M., Chen, Z.X., Feng, L.Q., Zhao, M., Xiao, H.: The impact of flow discharge
894 on the hydraulic characteristics of headcut erosion processes in the gully region of the Loess Plateau,
895 *Hydrological processes*, 34, 718-729, <https://doi.org/10.1002/hyp.13620>, 2020.

896 Shi, Q., Wang, W., Zhu, B., Guo, M.: Experimental study of hydraulic characteristics on headcut erosion and
897 erosional response in the tableland and gully regions of China, *Soil Science Society of America Journal*, 84,
898 700–716, <https://doi.org/10.1002/saj2.20068>, 2020.

899 Sidorchuk, A.: The potential of gully erosion on the Yamal peninsula, West Siberia. *Sustainability*, 12(1), 260,
900 <https://doi.org/10.3390/su12010260>, 2020.

901 Stein, O., Julien, P., Alonso, C.: Mechanics of jet scour downstream of a headcut, *Journal of Hydraulic Research*,
902 31, 723–738, <https://doi.org/10.1080/00221689309498814>, 1993.

903 Su, Z.A., Xiong, D.H., Dong, Y.F., Zhang, B.J., Zhang, S., Zheng, X.Y., Fang, H.D.: Hydraulic properties of
904 concentrated flow of a bank gully in the dry - hot valley region of southwest China, *Earth Surface Processes
905 and Landforms*, 40, 1351 - 1363. <https://doi.org/10.1002/esp.3724>, 2015.

906 Su, Z.A., Xiong, D.H., Dong, Y.F., Li, J.J., Yang, D., Zhang, J.H., He, G.X.: Simulated headward erosion of
907 bank gullies in the Dry-hot Valley Region of southwest China, *Geomorphology*, 204, 532–541,
908 <https://doi.org/10.1016/j.geomorph.2013.08.033>, 2014.

909 Sun, W.Y., Mu, X.M., Song, X.Y., Wu, D., Cheng, A.F., Qiu, B.: Changes in extreme temperature and
910 precipitation events in the Loess Plateau (China) during 1960–2013 under global warming, *Atmospheric
911 Research*, 168, 33-48, <https://doi.org/10.1016/j.atmosres.2015.09.001>, 2016.

912 Thompson, J.R.: Quantitative effect of watershed variables on rate of gully - head advancement. *Transactions
913 of the ASABE*, 7, 54 - 55, <https://doi.org/10.13031/2013.40694>, 1964.

914 Torri, D., Poesen, J.: A review of topographic threshold conditions for gully head development in different
915 environments, *Earth-Science Reviews*, 130, 73–85, <https://doi.org/10.1016/j.earscirev.2013.12.006>, 2014.

916 Valentin, C., Poesen, J., Li, Y.: Gully erosion: Impacts, factors and control, *Catena*, 63, 132–153,
917 <https://doi.org/10.1016/j.catena.2005.06.001>, 2005.

918 Vandekerckhove, L., Poesen, J., Govers, G.: Medium-term gully headcut retreat rates in southeast Spain
919 determined from aerial photographs and ground measurements, *Catena*, 50(2-4), 329-352,
920 [https://doi.org/10.1016/S0341-8162\(02\)00132-7](https://doi.org/10.1016/S0341-8162(02)00132-7), 2003.

921 Vandekerckhove, L., Poesen, J., Wijdenes, D.O., Nachtergaele, J., Tomás de Figueiredo.: Thresholds for gully
922 initiation and sedimentation in Mediterranean Europe, *Earth Surface Processes & Landforms*, 25(11), 1201-
923 1220, [https://doi.org/10.1002/1096-9837\(200010\)25:11<1201::AID-ESP131>3.0.CO;2-L](https://doi.org/10.1002/1096-9837(200010)25:11<1201::AID-ESP131>3.0.CO;2-L), 2015.

924 Vanmaercke, M., Poesen, J., Mele, B.V., Demuzere, M., Bruynseels, A., Golosov, V., Yermolaev, O.: How
925 fast do gully headcuts retreat?, *Earth - Science Reviews*, 154, 336 - 355,
926 <https://doi.org/10.1016/j.earscirev.2016.01.009>, 2016.

927 Vannoppen, W., Vanmaercke, M., De Baets, S., Poesen, J.: A review of the mechanical effects of plant roots on
928 concentrated flow erosion rates, *Earth - Science Reviews*, 150, 666 - 678,
929 <https://doi.org/10.1016/j.earscirev.2015.08.011>, 2015.

930 Vanwalleghem, T., Bork, H.R., Poesen, J., Schmidtchen, G., Dotterweich, M., Nachtergaele, J., Bork, H.,
931 Deckers, J., Brüsich, B., Bungeneers, J., De Bie, M.: Rapid development and infilling of a buried gully under
932 cropland, Central Belgium, *Catena*, 63, 221–243, <https://doi.org/10.1016/j.catena.2005.06.005>, 2005.

933 Vanwalleghem, T., Van Den Eeckhaut, M., Poesen, J., Deckers, J., Nachtergaele, J., Van Oost, K., Slenters, C.:
934 Characteristics and controlling factors of old gullies under forest in a temperate humid climate: a case study
935 from the Meerdaal Forest (Central Belgium), *Geomorphology*, 56(1), 15–29, <https://doi.org/10.1016/S0169->
936 555X(03)00043-6, 2003.

937 Wells, R.R., Alonso, C.V., Bennett, S.J.: Morphodynamics of Headcut Development and Soil Erosion in Upland
938 Concentrated Flows, *Soil Science Society of America Journal*, 73, 521–530.
939 <https://doi.org/10.2136/sssaj2008.0007>, 2009a.

940 Wells, R.R., Bennett, S.J., Alonso, C.V.: Effect of soil texture, tailwater height, and pore - water pressure on the
941 morphodynamics of migrating headcuts in upland concentrated flows, *Earth Surface Processes and Landforms*,
942 34, 1867 - 1877, <https://doi.org/10.1002/esp.1871>, 2009b.

943 Wells, R.R., Momm, H.G., Rigby, J.R., Bennett, S.J., Bingner, R.L., Dabney, S.M.: An empirical investigation
944 of gully widening rates in upland concentrated flows, *Catena*, 101, 114-121,
945 <https://doi.org/10.1016/j.catena.2012.10.004>, 2013.

946 Wen, X., Wu, X., Gao, M.: Spatiotemporal variability of temperature and precipitation in Gansu province
947 (northwest China) during 1951–2015, *Atmospheric Research*, 197, 132-149,
948 <https://doi.org/10.1016/j.atmosres.2017.07.001>, 2017.

949 Wen, Y., Kasielke, T., Li, H., Zhang, B., Zepp, H.: May agricultural terraces induce gully erosion? a case study
950 from the black soil region of northeast China. *Science of The Total Environment*, 750(4), 141715,
951 <https://doi.org/10.1016/j.scitotenv.2020.141715>, 2020.

952 Wu, Bing., Wang, Zhanli., Zhang, Qingwei., Shen, Nan., Liu, June., Wang, Sha.: Evaluation of shear stress and
953 unit stream power to determine the sediment transport capacity of loess materials on different slopes, *Journal of*
954 *Soil & Sediments*, 18, 116–127, <https://doi.org/10.1007/s11368-017-1758-5>, 2018.

955 Wu, B., Wang, Z., Shen, N., Wang, S.: Modelling sediment transport capacity of rill flow for loess sediments on
956 steep slopes, *Catena*, 147, 453-462, <https://doi.org/10.1016/j.catena.2016.07.030>, 2016.

957 Xia, L., Song, X.Y., Fu, N., Li, H.Y., Li, Y.L.: Impacts of land use change and climate variation on green water
958 in the Loess Plateau Gully Region—A case study of Nanxiaohegou basin, *Journal of Hydraulic Engineering*,
959 48(6), 678-688, (In Chinese), 2017.

960 Xu, J.Z., Li, H., Liu, X.B., Hu, W., Yang, Q.N., Hao, Y.F., Zhen, H.C., Zhang, X.Y.: Gully Erosion Induced by
961 Snowmelt in Northeast China: A Case Study, *Sustainability*, 11, <https://doi.org/10.3390/su11072088>, 2019.

962 Xu, X.M., Zheng, F.L., Wilson, G.V., Wu, M.: Upslope inflow, hillslope gradient and rainfall intensity impacts
963 on ephemeral gully erosion, *Land Degradation & Development*, 28, 2623-2635 <https://doi.org/10.1002/ldr.2825>,
964 2017.

965 Xu, X.M., Zheng, F.L., Qin, C., Wu, H.Y., Wilson, G.V.: Impact of cornstalk buffer strip on hillslope soil erosion
966 and its hydrodynamic understanding, *Catena*, 149, 417–425, <https://doi.org/10.1016/j.catena.2016.10.016>, 2017.

967 Xu, X.M., Wang, H.B., Zhao, J.Y., Liu, X.J.: Dynamic variation of soil erosion of Nanxiaohegou small
968 watershed during 2004-2016, *Soil and Water Conservation in China*, 443(2), 59-61, (In Chinese), 2019.

969 Yang, C.T.: Potential energy and stream morphology, *Water Resource Research*, 7(2), 311-223,
970 <https://doi.org/10.1029/WR007i002p00311>, 1971a.

971 Yang, C.T.: On river meanders, *Journal of Hydrology*, 13, 231-253, [https://doi.org/10.1016/0022-](https://doi.org/10.1016/0022-1694(71)90226-5)
972 1694(71)90226-5, 1971b.

973 Zhang, B.J., Xiong, D.H., Su, Z.A., Yang, D., Dong, Y.F., Xiao, L., Zhang, S., Shi, L.T.: Effects of initial step
974 height on the headcut erosion of bank gullies: a case study using a 3D photo-reconstruction method in the Dry-
975 hot Valley region of southwest China, *Physical Geography*, 37, 409–429,
976 <https://doi.org/10.1080/02723646.2016.1219939>, 2016.

977 Zhang, B.J., Xiong, D.H., Zhang G.H., Zhang, S., Wu, H., Yang, D., Xiao, L., Dong, Y.F., Su, Z.A., Lu, X.N.:
978 Impacts of headcut height on flow energy, sediment yield and surface landform during bank gully erosion
979 processes in the Yuanmou Dry - hot Valley region, southwest China, *Earth Surface Processes & Landforms*,
980 43(10), 2271-2282, <https://doi.org/10.1002/esp.4388>, 2018.

981 Zhang, H.X.: The characteristics of hard rain and its distribution over the Loess Plateau, *Acta Geographica*
982 *Sinica*, 38, 416–425, (In Chinese), 1983.

983 Zhang, G.H., Liu, Y.M., Han, Y.F., Zhang, X.C.: Sediment transport and soil detachment on steep slopes: I.
984 transport capacity estimation, *Soil Science Society of America Journal*, 73, 1291-1297,
985 <https://doi.org/10.2136/sssaj2008.0145>, 2009.

986 Zhang, X., Fan, J., Liu, Q., Xiong D.: The contribution of gully erosion to total sediment production in a small
987 watershed in Southwest China, *Physical Geography*, 39(3), 1-18,
988 <https://doi.org/10.1080/02723646.2017.1356114>, 2018.

989 Zhao, A.C.: Analysis of control models of typical small watershed in gully area of Loess Plateau, the east part
990 of Gansu Province, *Research of Soil and Water Conservation*, 1, 45–49, (In Chinese), 1994.

991 Zhu, T.X.: Gully and tunnel erosion in the hilly Loess Plateau region, China, *Geomorphology*, 153, 144–155,
992 <https://doi.org/10.1016/j.geomorph.2012.02.019>, 2012.